



**HAL**  
open science

## Are luminescent Ru 2+ chelated complexes selective coordinative sensors for the detection of heavy cations?

Christophe Gourlaouen, Benjamin Schweitzer, Chantal Daniel

### ► To cite this version:

Christophe Gourlaouen, Benjamin Schweitzer, Chantal Daniel. Are luminescent Ru 2+ chelated complexes selective coordinative sensors for the detection of heavy cations?. *Physical Chemistry Chemical Physics*, 2022, 24 (4), pp.2309-2317. 10.1039/D1CP04442G . hal-04016078

**HAL Id: hal-04016078**

**<https://hal.science/hal-04016078>**

Submitted on 6 Mar 2023

**HAL** is a multi-disciplinary open access archive for the deposit and dissemination of scientific research documents, whether they are published or not. The documents may come from teaching and research institutions in France or abroad, or from public or private research centers.

L'archive ouverte pluridisciplinaire **HAL**, est destinée au dépôt et à la diffusion de documents scientifiques de niveau recherche, publiés ou non, émanant des établissements d'enseignement et de recherche français ou étrangers, des laboratoires publics ou privés.



PCCP

**Are luminescent Ru<sup>2+</sup> chelated complexes selective coordinative sensors for the detection of heavy cations ?**

Journal:	<i>Physical Chemistry Chemical Physics</i>
Manuscript ID	CP-ART-09-2021-004442
Article Type:	Paper
Date Submitted by the Author:	27-Sep-2021
Complete List of Authors:	Gourlaouen, Christophe; CNRS, Laboratoire de Chimie Quantique; Strasbourg 1 University, Chemistry Schweitzer, Benjamin; Strasbourg 1 University Daniel, Chantal; CNRS, Chemistry; Strasbourg 1 University, Chemistry
Note: The following files were submitted by the author for peer review, but cannot be converted to PDF. You must view these files (e.g. movies) online.	
adf_struc.xyz gauss_struc.xyz	

SCHOLARONE™  
Manuscripts



Dr Chantal Daniel  
Laboratoire de Chimie Quantique  
Institut de Chimie Strasbourg  
UMR-7177 CNRS-UDS  
1 & 4 Rue Blaise Pascal  
67 070 Strasbourg Cedex France  
e-mail : gourlaouen@unistra.fr

Strasbourg September 24 2021

Phys Chem Chem Phys  
A journal of the RSC  
Editorial Office

Dear Editor, Dear Colleague,

You'll find enclosed a manuscript entitled "*Are luminescent Ru<sup>2+</sup> chelated complexes selective coordinative sensors for the detection of heavy cations ?*" submitted by Christophe Gourlaouen, Benjamin Schweitzer and Chantal Daniel to Phys Chem Chem Phys.

Motivated by a number of recent experimental articles claiming a high selectivity of Ru(II) complexes towards the specific detection of some metal cations in aqueous media we illustrate how quantum chemistry can contribute at validating or not the selectivity of a coordinative probe on the basis of calculated Gibbs free energies of complexation and computed structural, optical and photophysical properties.

In this work we show that in contrast to the conclusion of experimental findings by Kumar *et al* (Chem. Commun., 2014, 50, 8488), [Ru(bpy)<sub>2</sub>(bpym)]<sup>2+</sup> has not the optical and photophysical potential for a selective detection of Pd<sup>2+</sup> ions in water over a variety of other cations as proven by our analysis of the electronic transitions involved. However, the important work of Kumar combined to our study opens new perspective for experimentalists for the design of such probes.

I thank you for considering this article as publishable in *Phys Chem Chem Phys* as an article and I'm looking forward to hearing from you.

Sincerely yours

C. DANIEL, Research Director  
ICS Strasbourg  
Institut de Chimie

## ARTICLE

## Are luminescent Ru<sup>2+</sup> chelated complexes selective coordinative sensors for the detection of heavy cations ?

Received 00th January 20xx,  
Accepted 00th January 20xx

Christophe Gourlaouen,<sup>\*a</sup> Benjamin Schweitzer<sup>a</sup> and Chantal Daniel<sup>\*a</sup>

DOI: 10.1039/x0xx00000x

The ability of [Ru(bpy)<sub>2</sub>(bpym)]<sup>2+</sup> (bpy = 2,2'-bipyridine; bpym = 2,2'-bipyrimidine) at probing specifically heavy cations has been investigated by means of density functional theory for transition metals, group 12 elements and Pb<sup>2+</sup>. On the basis of calculated Gibbs free energies of complexation in water it is shown that all reactions are favorable with negative enthalpies excepted for Hg<sup>2+</sup>, the transition metal cations forming stable bi-metallic complexes by coordination to the bpym ligand. Comparison between the optical and photophysical properties of the Ru<sup>2+</sup> probe and those of the coordination compounds does not demonstrate a high selectivity due to very similar characteristics of the absorption and emission spectra. Whereas by complexation the lowest metal-to-ligand-charge-transfer (MLCT) shoulder of [Ru(bpy)<sub>2</sub>(bpym)]<sup>2+</sup> at 462 nm is more or less shifted to the red as function of the cation, the second MLCT band at 415 nm, less sensitive to the complexation, gains in intensity and is slightly blue-shifted. The visible MLCT emission of [Ru(bpy)<sub>2</sub>(bpym)]<sup>2+</sup> at 706 nm is altered by complexation leading to near IR (800-900 nm) emission in most of the coordination compounds. Complexation to some transition metal cations (Fe, Co, Rh and Pd) generates low-lying metal-centered (MC) excited states that quench luminescence. In contrast to the conclusion of experimental findings by Kumar *et al* (*Chem. Commun.* 2014, **50**, 8488-8490)<sup>1</sup>, [Ru(bpy)<sub>2</sub>(bpym)]<sup>2+</sup> cannot be proposed as fast and selective probe for monitoring Pd<sup>2+</sup> in aqueous media. Indeed, It does not possess the optical and photophysical characteristics necessary to discriminate Pd<sup>2+</sup> ions over a variety of other cations.

### 1 Introduction

Transition metal-based molecular chemosensors have been developed originally in order to combine emissive properties of organic fluorophores with the intrinsic properties of coordination compounds, namely selective and reversible binding, UV/visible absorption, and redox potential.<sup>2</sup> The idea was to follow the competition between photo-induced electron transfer (PET) / electronic energy transfer (EET) and fluorescence processes controlled by the environment, more particularly in term of the presence of metal ions or other chemical species of biological and environmental interest. In this context the emergence of metal-based supramolecular photochemistry<sup>3</sup> paved the way to the development of new compounds characterized by selective and reversible recognition, high sensitivity and a broad palette of efficient luminescent responses potentially competitive with intramolecular PET/EET.<sup>4</sup> Coordination to metal complex of an organic binding group dedicated to a specific analyte, encapsulation of lanthanides as sensitized photoactive centres or direct complexation of the analyte to the coordination compound are all approaches to achieve luminescent sensor molecules based on coordinated metals.<sup>5</sup> These pioneering strategies were then used for the developments of efficient probes employed in environmental, biological and clinical sciences.<sup>6</sup> The huge activity devoted to metal-organic

frameworks (MOFs) in the past decades resulted in highly selective multi-luminescent devices able to reversibly trap and probe a variety of analytes in a single molecular structure.<sup>7</sup> These developments take advantage of the specific host-guest interactions, the occurrence of PET processes as well as of the diversity of accessible excited states, namely metal-centred (MC), metal-to-ligand-charge-transfer (MLCT), ligand-to-ligand charge transfer (LLCT), ligand-to-metal-charge-transfer (LMCT) or ligand centred (LC). The presence of transition metal nodes associated to specific ligands gives to these multifunctional compounds the desired chemical reversibility, redox properties and electronic flexibility.<sup>8</sup> More recently, an improved knowledge of the rich photophysics of transition metal complexes characterized by efficient intersystem crossings (ISCs), long lifetimes, high luminescence quantum yields and large Stokes-shift concomitant to their structural and electronic flexibilities prompted new investigations of their chemosensing behavior.<sup>1,9</sup> Whatever the role of the transition metal-based coordination compound is in the sensing process, a detailed knowledge of its electronic structure and photophysics is mandatory in order to design efficient molecular chemosensor devices and to avoid an overestimation of their selectivity. Nowadays, quantum chemistry combined with efficient computational strategy could contribute at estimating the reactivity of the metal complex towards environment (solvent, cations, anions...) and at modelling realistic

absorption/emission properties.<sup>10</sup> In recent studies dedicated to pure organic chemosensors,<sup>11</sup> density functional theory (DFT) used in the context of transition metal-based molecular chemosensors, complements experiments for elucidating bonding structure and/or assigning excited states.<sup>12</sup> Most of the time deep analysis of the mechanisms underlying the chemosensing process is lacking.

The goal of this article is to illustrate how quantum chemistry can contribute at validating or not the selectivity of a coordinative probe. For this purpose, we have selected a promising Ru<sup>2+</sup> coordinative probe developed by Kumar et al<sup>1</sup> for a simple turn-on/turn-off detection of Pd<sup>2+</sup> via dual-optical analysis. The capability of [Ru(bpy)<sub>2</sub>(bpym)]<sup>2+</sup> (bpy = 2,2'-bipyridine; bpym = 2,2'-bipyrimidine) at probing specifically heavy cations is investigated by means of DFT and time-dependent (TD-DFT) for transition metals, group 12 elements and Pb<sup>2+</sup> and Ca<sup>2+</sup> on the basis of calculated complexation enthalpies, absorption and emission spectra in water.

## 2 Computational Details

Two series of calculations were performed. A first set of calculations was undertaken in order to compute the Gibbs free energy potential associated to the complexation of various [MCl<sub>x</sub>(H<sub>2</sub>O)<sub>n</sub>]<sup>q</sup> compounds (M= Ca<sup>2+</sup>, Mn<sup>2+</sup>, Fe<sup>2+</sup>, Co<sup>2+</sup>, Ni<sup>2+</sup>, Zn<sup>2+</sup>, Rh<sup>3+</sup>, Pd<sup>2+</sup>, Cd<sup>2+</sup>, Pt<sup>2+</sup>, Au<sup>+</sup>, Au<sup>3+</sup>, Hg<sup>2+</sup>, Pb<sup>2+</sup>; x=1-3; n=0-4; q=0,+1) to [Ru(bpy)<sub>2</sub>(bpym)]<sup>2+</sup> using GAUSSIAN 09 quantum chemistry package.<sup>13</sup>

These calculations were carried out at the DFT level of theory with the B3LYP functional including dispersion corrections<sup>14</sup> and using the 6-31+G\*\* basis set<sup>15</sup> for C, N and O and the Stuttgart-Dresden SDD basis sets and associated small core pseudopotentials for metal atoms.<sup>16</sup> Solvation (water) was included through a PCM model.<sup>17</sup> Geometry optimizations were performed within the less constrained symmetry. Thermochemistry and stationary state analysis were extracted from the frequency calculations.

A second set of calculations was performed using ADF2019 software.<sup>18</sup> The structures of [Ru(bpy)<sub>2</sub>(bpym)]<sup>2+</sup> **1** and [Ru(bpy)<sub>2</sub>(bpym)M(Cl)<sub>n</sub>]<sup>2+</sup> **1-M** (M= Ca<sup>2+</sup>, Mn<sup>2+</sup>, Fe<sup>2+</sup>, Co<sup>2+</sup>, Ni<sup>2+</sup>, Zn<sup>2+</sup>, Rh<sup>3+</sup>, Pd<sup>2+</sup>, Cd<sup>2+</sup>, Pt<sup>2+</sup>, Au<sup>+</sup>, Au<sup>3+</sup>, Hg<sup>2+</sup>, Pb<sup>2+</sup>) depicted in Figure 1 for M=Pd have been fully optimized at the DFT/B3LYP level associated to TZP, triple- $\zeta$  basis sets<sup>19</sup> on all atoms and including dispersion corrections. Scalar relativistic corrections

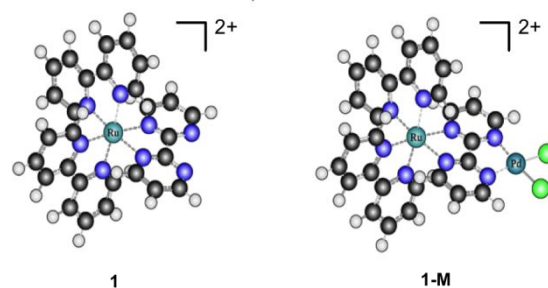


**Figure 1.** Structure of **1** [Ru(bpy)<sub>2</sub>(bpym)]<sup>2+</sup> (bpy = 2,2'-bipyridine; bpym = 2,2'-bipyrimidine) (left) and **1-M** (M = Pd) for [Ru(bpy)<sub>2</sub>(bpym)]<sup>2+</sup> coordinated to PdCl<sub>2</sub> (right).

were incorporated through the zero-order relativistic approximation (ZORA)<sup>20</sup> including solvent corrections by means of the Conductor-like Screening Model COSMO<sup>21</sup> of water ( $\epsilon = 78.4$ ). The theoretical absorption spectra were computed by means TD-DFT<sup>22</sup> performed on the ground state optimized structures. The spin-orbit coupling (SOC) has been included at a perturbative level.<sup>23</sup> The Tamm-Dancoff approximation (TDA)<sup>24</sup> was used to avoid over stabilization of the lowest triplet states. The low-lying singlet and triplet electronic excited states were optimized at the same level of theory using TD-DFT procedure available in ADF. The character of the electronic excited states contributing significantly to the absorption and emission spectra have been analysed with TheoDOR.<sup>25</sup>

## 3 Complexation: structures and energetics

### 3.1 Structures

In order to estimate the selectivity of the salt complexation onto **1** and to evaluate the complexation Gibbs free energies, we optimized separately **1** and the aqueous salt (e.g. [Pd(Cl)<sub>2</sub>(OH<sub>2</sub>)<sub>2</sub>]). The number of water molecules around the cation and its spin state has to be considered in the calculation conditions. For Pd<sup>2+</sup> and Pt<sup>2+</sup> cations (d<sup>8</sup> species), we selected square-planar structures with two chloride anions and two water molecules, both in trans position (Figure 2), the closed singlet being the electronic ground state configuration. The Ni<sup>2+</sup> cation behaves differently, with a triplet electronic ground state in an octahedral conformation, the chloride anions being in apical positions (Figure 2). The Au<sup>3+</sup> cation gives rise to a square planar complex with three chloride anions and one water molecule (Figure 2). The d<sup>10</sup> cations (Zn<sup>2+</sup>, Cd<sup>2+</sup> and Hg<sup>2+</sup>) do not exhibit any stable structures with water molecules in the first shell leading to [M(Cl)<sub>2</sub>] salts. The Ca<sup>2+</sup>, Mn<sup>2+</sup>, Fe<sup>2+</sup> and Co<sup>2+</sup> adopt an octahedral structure, general formula [M(Cl)<sub>2</sub>(OH<sub>2</sub>)<sub>4</sub>] with the chlorine anion occupying the apical positions associated to singlet ground state for Ca<sup>2+</sup> and Fe<sup>2+</sup>, a quartet ground state for Co<sup>2+</sup> and a sextet ground state for Mn<sup>2+</sup>. Rh<sup>3+</sup> also adopt an octahedral arrangement. The environment of Pb<sup>2+</sup> is a cis-divacant distorted octahedron, the so-called see-saw structure.<sup>26</sup>

Upon complexation with **1**, the Pd<sup>2+</sup> and Pt<sup>2+</sup> aqueous compounds release two water molecules whereas the Au(III) aqueous compound loses one water and one chlorine anion to form square planar structures with the chlorine in cis positions. The Zn<sup>2+</sup>, Cd<sup>2+</sup> and Hg<sup>2+</sup> cations adopt a distorted tetrahedral structure around M. The d<sup>10</sup> Au<sup>+</sup> cation releases one water molecule and affords bonding with a single nitrogen of the bipyrimidine. The Pb<sup>2+</sup> cation expels the water molecules upon complexation kipping its see-saw structure.

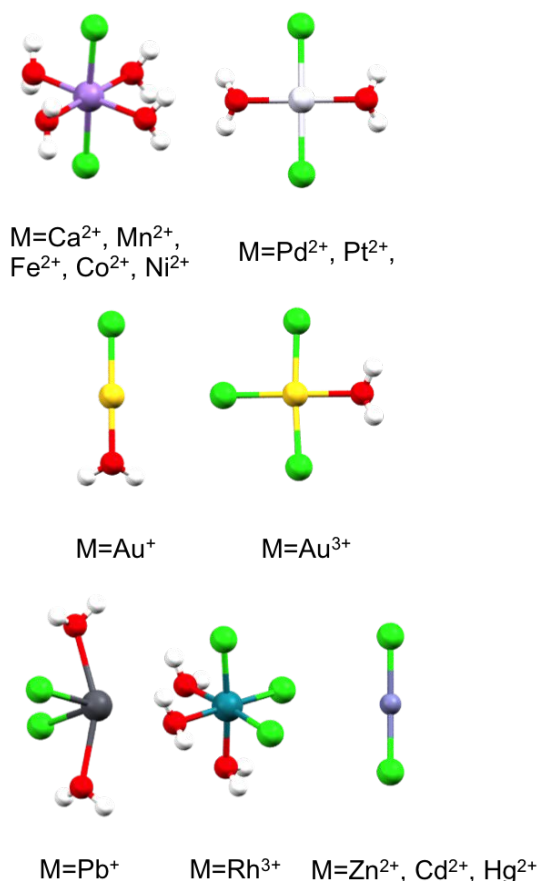


**Figure 2.** Optimized structures of the [MCl<sub>x</sub>(H<sub>2</sub>O)<sub>n</sub>] compounds (M=Ca<sup>2+</sup>, Mn<sup>2+</sup>, Fe<sup>2+</sup>, Co<sup>2+</sup>, Ni<sup>2+</sup>, Zn<sup>2+</sup>, Rh<sup>3+</sup>, Pd<sup>2+</sup>, Cd<sup>2+</sup>, Pt<sup>2+</sup>, Au<sup>+</sup>, Au<sup>3+</sup>, Hg<sup>2+</sup>, Pb<sup>2+</sup>; x=1-3; n=0-4).

The cations Ca<sup>2+</sup>, Mn<sup>2+</sup>, Co<sup>2+</sup>, Fe<sup>2+</sup>, Ni<sup>2+</sup> and Rh<sup>3+</sup> retain their octahedral structures with the departure of two equatorial water molecules. All these complexes have +2 global charge coming from **1** and have a singlet ground state, except **1-Ni** that has a triplet ground state, **1-Co** is a quartet and **1-Mn** is a sextet. Au<sup>3+</sup> forms square planar species upon complexation with **1**, one chlorine anion having to leave to form **1-Au(III)** in a singlet electronic ground state with a net charge of +3 in contrast to all the other ones.

Some important optimized bond distances and angles of **1** and **1-M**, the structures of which are given in the SI section, are reported in Table 1. The Ru-N distances, including that of the bipyrimidine, are scarcely affected by complexation of M (Table 1), they increase from 2.085 Å in **1** to 2.102 Å in **1-Au(III)**. The M-N distances are much more dependent of M as

are the M-O and M-Cl distances. As mentioned earlier, the d<sup>10</sup> cations form weak complexes. The **1-Hg** complex is characterized by a long Hg-N distance of 3.556 Å (Table 1).

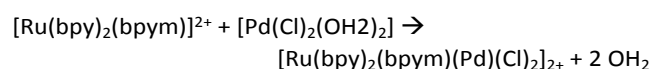
In **1-Au(I)**, the values of the Au-N distances confirm that only one nitrogen atom is bonded to the cation. Similarly, in **1-Pb** there is a clear difference between the two Pb-N and Pb-Cl distances: for both there is one short and one long bond length. This is due to the seesaw structure. In such structure, (Figure 2), one Cl<sup>-</sup> anion has a nitrogen atom in trans position, the second Cl<sup>-</sup> has no ligand in the trans position. The situation is the same for the nitrogen atoms. The two atoms (one Cl<sup>-</sup> and one nitrogen) repel each other leading to longer Pb-Cl and Pb-N bond lengths than for the two atoms, which have no trans partner. This trans repulsion is further illustrated by the N-Pb-Cl angle that is significantly smaller than 180°. It is of 146.7° in **1-Pb**.

**Table 1.** Selected optimized bond distances (in Å) and bond angles (in °) of the complexes **1-M**. Experimental values known for **1-Pd**<sup>1</sup> are given in parenthesis.

Complex	M-Cl	M-O	M-N	Cl-M-Cl
<b>1-Ca</b>	2.705, 2.722	2.440, 2.446	2.607, 2.610	133.2
<b>1-Mn</b>	2.455, 2.455	2.284, 2.284	2.361, 2.361	166.5
<b>1-Fe</b>	2.355, 2.355	2.048, 2.048	1.975, 1.975	172.7
<b>1-Co</b>	2.395, 2.412	2.172, 2.185	2.157, 2.196	172.9
<b>1-Ni</b>	2.408, 2.408	2.187, 2.187	2.169, 2.169	170.6
<b>1-Zn</b>	2.238, 2.249		2.204, 2.024	137.7
<b>1-Rh</b>	2.343, 2.366,	2.142	2.089, 2.089	93.9
	2.367			92.2
<b>1-Pd</b>	2.330, 2.330		2.089, 2.089	92.2
	(2.231, 2.280)		(1.939, 2.049)	(92.3)
<b>1-Cd</b>	2.492, 2.492		2.546, 2.546	152.4
<b>1-Pt</b>	2.351, 2.351		2.068, 2.068	91.4
<b>1-Au(I)</b>	2.330		2.137, 2.849	
<b>1-Au(III)</b>	2.313, 2.313		2.113, 2.113	90.7
<b>1-Hg</b>	2.453, 2.453		3.556, 3.556	171.2
<b>1-Pb</b>	2.658, 2.711		2.711, 2.889	93.4

### 3.2 Solvated metal cation complexation

The balance chemical equation corresponding to the complexation of **1** by solvated metal compounds is given by,



where the water molecules are substituted by the Ru<sup>2+</sup> complex **1**, as illustrated above for the palladium cation. The spin and symmetry characteristics of the solvated metal compounds are reported in Table 2 for the series under study here.

**Table 2.** Spin state of  $[MCl_x(H_2O)_n]^q$  ( $M = Ca^{2+}, Mn^{2+}, Fe^{2+}, Co^{2+}, Ni^{2+}, Zn^{2+}, Rh^{3+}, Pd^{2+}, Cd^{2+}, Pt^{2+}, Au^+, Au^{3+}, Hg^{2+}, Pb^{2+}; x=1-3; n=0-4; q=0,+1$ ) and Gibbs free energy  $\Delta G$  (in  $\text{kJ Mol}^{-1}$ ) of complexation of **1** with them.

Metal compound	Spin state	$\Delta G$
$[Ca(Cl)_2(OH_2)_4]$	0	-27.5
$[Mn(Cl)_2(OH_2)_4]$	5/2	-40.7
$[Fe(Cl)_2(OH_2)_4]$	0	-87.6
$[Co(Cl)_2(OH_2)_4]$	3/2	-59.5
$[Ni(Cl)_2(OH_2)_4]$	1	-67.2
$[Zn(Cl)_2]$	0	-17.0
$[Rh(Cl)_3(OH_2)_3]$	0	-113.5
$[Pd(Cl)_2(OH_2)_2]$	0	-108.6
$[Cd(Cl)_2]$	0	+19.2
$[Pt(Cl)_2(OH_2)_2]$	0	-149.7
$[Au(Cl)(OH_2)]$	0	-44.5
$[Au(Cl)_3(OH_2)]$	0	-8.6
$[Hg(Cl)_2]$	0	+23.0
$[Pb(Cl)_2(OH_2)]$	0	-36.1

Complexation occurs via coordination of the cation to the bpy ligand of complex **1**. As illustrated by the energetics reported in Table 2 and other than  $[Cd(Cl)_2]$  and  $[Hg(Cl)_2]$ , negative Gibbs free energies characterize the complexation reaction for all investigated compounds. Clearly complexation of 2<sup>nd</sup> and 3<sup>rd</sup>-row cations (groups 9 and 10) to **1** is more favourable than the complexation of 1<sup>st</sup>-row transition metal cations with  $|\Delta G| > 100.0 \text{ kJ Mol}^{-1}$  for  $Rh^{3+}$ ,  $Pd^{2+}$ ,  $Pt^{2+}$  and  $40.0 < |\Delta G| < 90.0 \text{ kJ Mol}^{-1}$  for  $Mn^{2+}$ ,  $Fe^{2+}$ ,  $Co^{2+}$  and  $Ni^{2+}$ . The  $d^{10}$  and  $d^0$  compounds are either weakly bounded ( $Zn^{2+}$  and  $Ca^{2+}$ ,  $|\Delta G| < 40.0 \text{ kJ Mol}^{-1}$ ) or not ( $Cd^{2+}$  and  $Hg^{2+}$ ) (Table 2). **1-Au(I)** complex has an intermediate complexation value close to that of the 1<sup>st</sup>-row cations. The case of **1-Au(III)** complex is special. Indeed, one chlorine anion, along with the water molecule, has to be expelled from the coordination sphere in order to keep the square planar structure around the  $Au^{3+}$  cation. This loss of one anion replace by a neutral ligand leads to a rather low complexation energy although it remains negative. These results exemplify the lack of selectivity as far as the complexation process is concerned leading to stable  $[Ru(bpy)_2(bpym)M(Cl)_n]^{2+}$  complexes with  $M$  being a heavy transition metal element.

## 4 Optical properties

### 4.1 Absorption spectra

The TD-DFT absorption spectra of **1** and **1-Pd** are depicted in Figure 3, the individual calculated absorption spectra of the other **1-M** complexes being represented in Figures S1-S15 (SI section). The calculated transition energies, electronic composition of the states and associated oscillator strengths can be found in Tables S1-S15 (SI Section).

The theoretical absorption spectrum of **1** reproduces rather well the experimental features with a first band between 350-500 nm with a maximum at 415 nm vs. an experimental value of 428 nm and a shoulder at about 462 nm vs. 480 nm experimentally. As illustrated by the analysis of the singlet electronic excited states assigned to this visible band (Figure 4), the MLCT character originating from the ruthenium (thereafter  $M_{Ru}LCT$ ) is preponderant with minor contributions of ligand centered (LC) and ligand-to-ligand-charge-transfer (LLCT) transitions. The intense band calculated between 225 and 325 nm is attributed to LC transitions on the bpy and bpym ligands (Table S1). No metal-centered (MC) state on the ruthenium ( $MC_{Ru}$ ) are present at low energy.

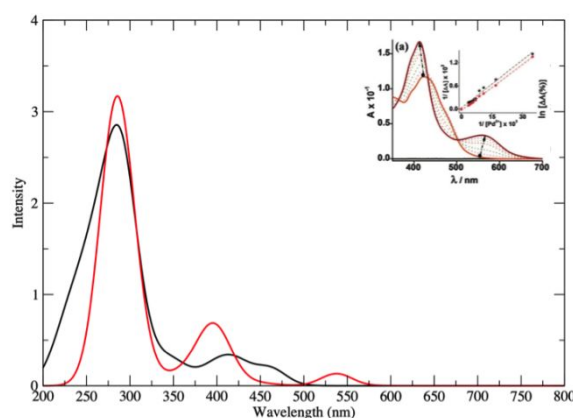


**Figure 3.** TD-DFT absorption spectra of **1** (in black) and **1-Pd** (in red) in water without SOC. The experimental spectrum<sup>1</sup> of **1** (in orange) and of **1-Pd** (dark red) is reproduced in the inset for comparison.

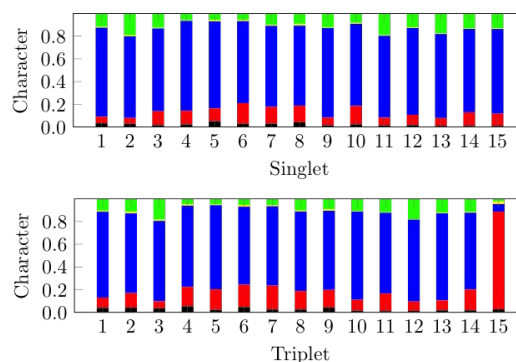


**Figure 4.** Character of the low-lying triplet states (T1-T15) and of the low-lying singlet states (S1-S15) of **1** contributing to the lowest absorption band calculated between 350-500 nm with the following color code: blue for  $M_{Ru}LCT$ ; green for LLCT; red for LC; black for  $MC_{Ru}$ .

The low-lying triplet states possess a major  $M_{Ru}LCT$  character (Figure 4) and their composition does not differ significantly from those of the corresponding singlets. Including SOC has no

effect on the absorption spectra of **1** and **1-Pd** (Figures S1 and S9).

Whereas the upper intense band (225-325 nm) of **1** is not really affected by complexation, the lowest band is split into two parts (Figure 3). The first one of  $M_{Ru}L_{bpy}CT$  character is shifted to the red with a new band calculated at 538 nm and experimentally observed at 565 nm. This is a direct effect of the coordination to the *bpy*m ligand, the acceptor character of which is enhanced by complexation. The second band  $M_{Ru}L_{bpy}CT/M_{Ru}L_{bpy}CT$  is slightly shifted to the blue and gains in intensity because of the contribution of three transitions calculated at 390, 392 and 404 nm with significant oscillator strengths. As shown by the composition of the low-lying singlet and triplet excited states in **1-Pd** (Figure 5), the density and diversity of excited state increases dramatically by complexation developing a high degree of mixing. However, the  $M_{Ru}LCT$  states remain the only ones having oscillator strength in the visible energy domain.

Complexation generates low-lying metal-to-metal-charge-transfer ( $M_{Ru}M_{Pd}CT$ ) transitions (Figure 5), which do not contribute to the absorption spectrum.

The simulated absorption spectrum of **1-Pt** is very similar to the one of **1-Pd** (Figure 6) three maxima at 540 nm, 390 nm and 280 nm assigned to  $ML_{bpy}CT$ ,  $ML_{bpy/bpy}CT$  and LC, respectively. As in **1-Pd**, SOC does not affect the absorption spectra of **1-Pt**, which is dominated by contribution from the ligands or the ruthenium.

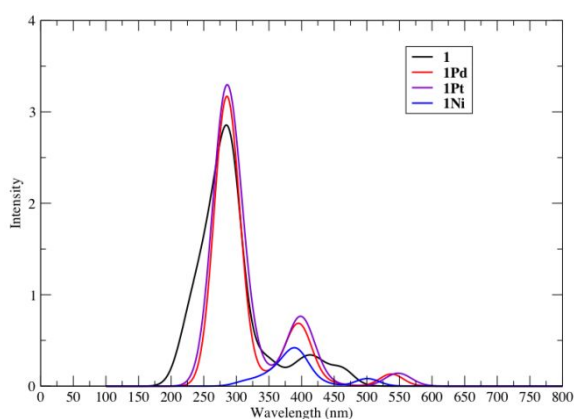


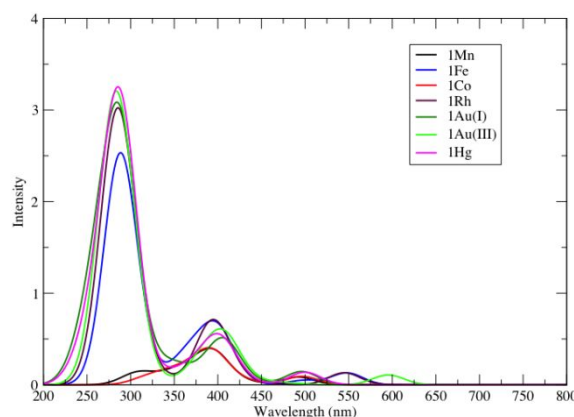
**Figure 6.** TD-DFT absorption spectra of **1** (in black), **1-Pd** (in red), **1-Pt** (in purple) and **1-Ni** (in blue) in water without SOC.

**Figure 5.** Character of the low-lying singlet (S1-S30) and triplet excited (T1-T30) states of **1-Pd** with the following color code: blue for  $M_{Ru}LCT$ ; green for  $LLCT$ ; red for  $LC$ ; black and grey for  $MC$  (Ru or Pd); pink for  $XLCT$ ; yellow for  $M_{Pd}LCT$ ; orange for  $XM_{Pd}CT$ ; violet for  $M_{Ru}M_{Pd}CT$ ; teal for other transitions.

A comparative analysis of the excited state composition of **1-Pt** (Table S9 and S11) and **1-Pd** (Figure 5) confirms that the complexation of **1** by  $Pd^{2+}$  and  $Pt^{2+}$  results in nearly coincident absorption spectra not sensitive selectively to one or the other cation. The **1-Ni** complex exhibits low-lying  $MC$  states with very low oscillator strengths. Whereas these states do not contribute to the absorption, the  $ML_{bpy}CT$  and  $ML_{bpy/bpy}CT$  transitions are assigned to the two lowest bands at 500 nm and 380 nm, similarly to **1-Pd** and **1-Pt**.

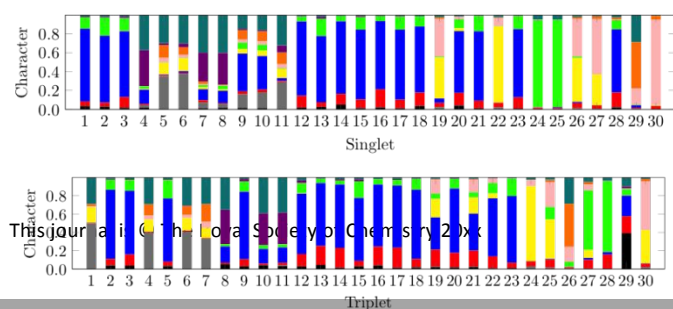
The calculated absorption spectra of **1-Ca**, **1-Zn** and **1-Pb** (Figures S2, S7 and S15) exhibit similar features to that of **1-Pd** (Figure S9). However, the nature of the transitions is close to that of **1** with no contribution of the M cation to the electronic transitions.

Figure 7 represents the calculated absorption spectra generated by the complexation of **1** with transition metal cations, namely **1-Mn**, **1-Fe**, **1-Co**, **1-Rh**, **1-Au(I)**, **1-Au(III)** and the one of **1-Hg**. All spectra generated by complexation of **1** reveal a three-band structure as observed in the complexes discussed above except that of **1-Fe**. The calculated transition energies, electronic composition of the states and associated oscillator strengths can be found in Tables S3 to S14 (SI Section).



**Figure 7.** TD-DFT absorption spectra **1-Mn** (in black), **1-Fe** (in blue), **1-Co** (in red), **1-Rh** (in purple), **1-Au(I)** (in dark green), **1-Au(III)** (in light green) and **1-Hg** (in magenta) in water without SOC.

The lowest band attributed to  $M_{Ru}L_{bpy}CT$  (**1-Mn**, **1-Co**, **1-Rh**, **1-Au(I)**, **1-Au(III)**, **1-Hg**) or  $M_{Fe}L_{bpy}CT$  (**1-Fe**) (Figure 7) is sensitive to the metal cation with an important red-shift, as compared to the lowest shoulder of **1** calculated 462 nm, for  $Au^{3+}$  (S6, 595 nm), less important in the case of  $Rh^{3+}$  (S3, 545 nm). It is moderate for the other cations with a shoulder at about 500 nm, S7 at 492 nm for  $Mn^{2+}$ , S9 at 499 nm for  $Fe^{2+}$ , S12 at 496 nm for  $Co^{2+}$ , S3 at 510 nm for  $Cd^{2+}$ , S3 at 496 nm for  $Au^+$  and S3 at 500 nm for  $Hg^{2+}$ . The spectra of **1-Fe** differ from the previous ones by the presence of a  $M_{Fe}L_{bpy}CT$  electronic





transition (S7) at 548 nm, more intense than the  $M_{RuLbpy}CT$  transition. According to our calculations, this is the only observed influence of the metal cation on one of the absorption spectra.

The character of the transitions associated to the low-lying singlet excited states (S1-S20) contributing to the absorption between 350 nm and 600 nm (Figure S18) points to the dominance of low-lying MC and  $M_{FeLbpy}CT/M_{FeLbpy}CT$  states in the iron coordinated complex whereas the spectra of  $Au^+$  and  $Hg^{2+}$  containing complexes are nearly pure  $M_{RuLbpy/bpym}CT$  as in **1** (Figures S20 and S22). The compounds generated by complexation with  $Au^{3+}$  and  $Rh^{3+}$  are characterized by a high density of mixed states (Figures S19 and S21). The absorption spectrum of **1-Rh** exhibits low-lying singlet states with  $MC_{Rh}$  and  $M_{Ru}M_{Rh}CT$  contributions and several halide-to-ligand-charge-transfer (XLCT) states. Electronic transitions with mixed contributions characterize the absorption spectrum of **1-Au(III)** with either  $M_{Ru}M_{Au}CT$  character in S1, S2 or S3 or  $XM_{Au}CT$  character at higher energy (S10, S12, S13 or S17). It is noteworthy to point out that, whatever the complex is, the  $M_{RuLbpy}CT$  contributions are nearly unaffected by the nature of the cations, which does not contribute to the absorption (except for **1-Fe**) and the first strongly absorbing state is the 3<sup>rd</sup>  $M_{RuLbpy}CT$ , more or less shifted.

#### 4.2 Low lying singlet and triplet states

In order to get insight into the emissive properties of the complexes under investigation the lowest triplet excited states have been fully optimized in water. The calculated emission wavelengths of T1 and T2 are reported in Table 3 and Table 4 as well as the character, deformation and stabilization energies corresponding to the minima of the associated potential energy surfaces (PES). The emission wavelengths corresponding to the S1 optimized structure have been calculated only for **1** and **1-Pd** leading to  $\lambda^{em}$  values of 645 nm

The calculated S1 and T1 emission wavelengths of **1**, namely 645 nm and 706 nm, respectively are within the domain of experimental emission of the complex at about 670 nm.<sup>1</sup> Both the singlet and the triplet are characterized as MLCT states. Together **1-Pd**, **1-Pt** and **1-Ni** possess low-lying T1 and T2 triplet structures, the first one of MLCT character emitting at ~ 880 nm, meaning a significant red-shift by complexation as compared to **1**. However, the presence of the T2 MC state in these complexes has different consequences as far as the emission is concerned. In the case of **1-Ni** and **1-Pd** the deformation and stabilization energies (Table 3) support a luminescence quenching by this MC state calculated around 1500 nm in agreement with what is observed experimentally.<sup>1</sup> In contrast, the  $E_{def}$  and  $E_{stab}$  values associated to the **1-Pt** complex (Table 3) are in favor of an efficient luminescence at 889 nm, not observable within the domain of energy explored by the experiments, namely (600-800 nm), supposed to prove a high degree of selectivity.<sup>1</sup> Similarly, the emissive signal at 670 nm is red-shifted in the case of **1-Ca** (791 nm), **1-Zn** (858 nm) and **1-Pb** (809 nm) complexes for which there is no competition with MC states.

The lowest T1 state of **1-Fe** and **1-Co** correspond to MC states calculated in the far infrared, whereas **1-Mn**, **1-Cd**, **1-Au(I)** and **1-Hg** are characterized by low-lying MLCT states emitting between 790 nm and 900 nm.  $Ru^{2+}$  to  $Au^{3+}$  charge transfer (T1/S0 PES crossing) quenches the potential emission of **1-Au(III)** via T1. The  $M_{Ru}LCT$  and  $M_{Rh}C$  states are almost degenerate and are in competition in **1-Rh**. However, the emission wavelength computed for those states also lead to a strong red shift compared to **1**.

**Table 3.** Character, deformation ( $E_{def}$ ), emission ( $E_{em}$ ), stabilization ( $E_{stab}$ ) energies (in eV) and  $\lambda^{em}$  (in nm) associated to the lowest T1 excited states of **1**, **1-Pd**, **1-Pt**, **1-Ni**, **1-Ca**, **1-Zn** and **1-Pb** and lowest S1 state of **1**.

	<b>1</b>	<b>1-Pd</b>	<b>1-Pt</b>	<b>1-Ni</b>
	T <sub>1</sub>	T <sub>2</sub>	T <sub>1</sub>	T <sub>2</sub>
Character	$M_{Ru}LCT$	$M_{Ru}LCT$	MC(Pd)	$M_{Ru}LCT$
$E_{def}$	0.27	0.26	0.53	0.24
$E_{em}$	1.76	1.41	0.81	1.39
$E_{stab}$	2.02	1.66	1.33	1.63
$\lambda^{em}$	706	880	1533	889
	T <sub>1</sub>	T <sub>2</sub>	T <sub>1</sub>	T <sub>2</sub>
Character	$M_{Ru}LCT$	MC(Pt)	$M_{Ru}LCT$	$M_{Ru}LCT$
$E_{def}$	0.27	1.80	0.26	0.66
$E_{em}$	1.76	0.24	1.54	0.82
$E_{stab}$	2.02	2.04	1.80	1.48
$\lambda^{em}$	706	806	1520	

	<b>1</b>	<b>1-Ca</b>	<b>1-Zn</b>	<b>1-Pb</b>
	T <sub>1</sub>			
Character	$M_{Ru}LCT$	$M_{Ru}LCT$	$M_{Ru}LCT$	$M_{Ru}LCT$
$E_{def}$	0.27	0.27	0.25	0.25
$E_{em}$	1.76	1.57	1.44	1.53
$E_{stab}$	2.02	1.84	1.69	1.78
$\lambda^{em}$	706	791	858	809

a) These values are qualitative because of convergence problems

and 822 nm, respectively.

### 4.3 Optical selectivity

The first and second absorption peaks and the calculated emission wavelengths associated to the lowest T1 triplet state of the **1-M** complexes are reported in Table 5 for comparison. The selectivity of the response of **1** upon complexation with various metal cations is governed by three factors, namely the complexation energy, the perturbation of the absorption spectrum and the alteration of emissive properties. On this

**Table 4.** Character, deformation ( $E_{\text{def}}$ ), emission ( $E_{\text{em}}$ ), stabilization ( $E_{\text{stab}}$ ) energies (in eV) and  $\lambda^{\text{em}}$  (in nm) associated to the lowest T1 excited states of **1-Mn**, **1-Fe**, **1-Co**, **1-Rh**, **1-Cd**, **1-Au(I)**, **1-Au(III)** and **1-Hg** and T2 state of **1-Rh**.

	Character	$E_{\text{def}}$	$E_{\text{em}}$	$E_{\text{stab}}$	$\lambda^{\text{em}}$
<b>1-Mn</b>	$M_{\text{Ru}}\text{LCT}$	0.26	1.55	1.81	798
<b>1-Fe</b>	$\text{MC}(\text{Fe})$	0.11	0.50	0.61	2498
<b>1-Co</b>	$\text{MC}(\text{Co})$	0.06	0.23	0.29	5411
<b>1-Rh</b>	$M_{\text{Ru}}\text{LCT}$	0.28	1.37	1.65	904
	$\text{MC}(\text{Rh})$	0.73	0.88	1.60	1412
<b>1-Cd</b>	$M_{\text{Ru}}\text{LCT}$	0.25	1.49	1.74	834
<b>1-Au(I)</b>	$M_{\text{Ru}}\text{LCT}$	0.25	1.56	1.81	792
<b>1-Au(III)<sup>a</sup></b>	$M_{\text{Ru}}\text{MCT}$	0.30	-	0.30	-
<b>1-Hg</b>	$M_{\text{Ru}}\text{LCT}$	0.10	1.56	1.66	797

basis, to be selective, the complex should bind preferentially the  $\text{Pd}^{2+}$  salt and exhibit specific optical responses. The absorption spectrum of **1** is dominated by  $M_{\text{Ru}}\text{LCT}$  states in the first absorbing band and by LC states in the second main absorbing band. The emission originates from the lowest triplet state corresponding to the  $M_{\text{Ru}}\text{LCT}$  transition to the bipyrimidine. The present calculations show that coordination of complex **1** to almost all considered cations is favourable, some of them being potentially competitive with  $\text{Pd}^{2+}$ .  $\text{Pt}^{2+}$  and  $\text{Rh}^{3+}$  give one illustration, their binding energies being greater than the one calculated for  $\text{Pd}^{2+}$ . The complexation is not specific to  $\text{Pd}^{2+}$ .

The optical response of **1** to complexation with  $\text{Pd}^{2+}$  is the splitting of the first absorbing band. The  $M_{\text{Ru}}\text{LCT}$  shoulder observed in the absorption spectrum of **1** is strongly red shifted (around 70 nm) in **1-Pd**. This shift results from the greater electrophilicity of the ligand but not from a direct contribution of the  $\text{Pd}^{2+}$  cation to the transition. Similar feature is observed for all other cations. In all cases, the first absorbing band is shifted towards the red, the shift depending

on the cation nature. Consequently, several complexes absorb in the same domain of energy than **1-Pd** (**1-Pt**, **1-Rh** and **1-Fe**, Table 5) making the change of absorption spectrum nonspecific to **1-Pd**.

The quenching of the luminescence in the visible energy domain observed in **1-Pd** is due to the relaxation of the complex into a  $M_{\text{Cpd}}$  state found to be the global minimum of the lowest triplet potential energy surface. More generally, nearly all investigated complexes are characterized by a  $M_{\text{Ru}}\text{LCT}$  emission in the infra-red domain (800-900nm) ( $\text{Ca}^{2+}$ ,  $\text{Mn}^{2+}$ ,  $\text{Zn}^{2+}$ ,  $\text{Cd}^{2+}$ ,  $\text{Pt}^{2+}$ ,  $\text{Au}^+$ ,  $\text{Hg}^{2+}$ ,  $\text{Pb}^{2+}$ ). One complex is not emissive due to the crossing between the triplet PES ( $\text{Au}^{3+}$

**Table 5.** Calculated absorption and emission wavelengths (in nm) of **1-M** complexes and character associated to the emissive state.

	$\lambda^{\text{abs}}(1)$	$\lambda^{\text{abs}}(2)$	$\lambda^{\text{em}}$	State character
<b>1</b>	462	415	706	$M_{\text{Ru}}\text{LCT}$
<b>1-Ca</b>	495	403, 399	791	$M_{\text{Ru}}\text{LCT}$
<b>1-Mn</b>	492	396, 392	798	$M_{\text{Ru}}\text{LCT}$
<b>1-Fe</b>	548	401, 396,	2498	$M_{\text{Fe}}\text{C}$
		392		
<b>1-Co</b>	496	395, 391	5411	$M_{\text{Co}}\text{C}$
<b>1-Ni</b>	501	394, 393	-	$M_{\text{Ni}}\text{C}$
<b>1-Zn</b>	515	391, 387,	858	$M_{\text{Ru}}\text{LCT}$
		382		
<b>1-Rh</b>	545	404, 402,	1412	$M_{\text{Rh}}\text{C}$
		392		
<b>1-Pd</b>	538	404, 392,	1533	$M_{\text{Pd}}\text{C}$
		390		
<b>1-Cd</b>	510	399, 397	834	$M_{\text{Ru}}\text{LCT}$
<b>1-Pt</b>	548	407, 392,	889	$M_{\text{Ru}}\text{LCT}$
		391		
<b>1-Au(I)</b>	496	404, 402	792	$M_{\text{Ru}}\text{LCT}$
<b>1-Au(III)</b>	595	408	-	$M_{\text{Ru}}M_{\text{Au}}\text{CT}$
<b>1-Hg</b>	500	400	797	$M_{\text{Ru}}\text{LCT}$
<b>1-Pb</b>	498	414, 400,	809	$M_{\text{Ru}}\text{LCT}$
		397		

with a  $M_{\text{Ru}}M_{\text{Au}}\text{CT}$  state) and the electronic ground state, whereas the others ( $\text{Fe}^{2+}$ ,  $\text{Co}^{2+}$ ,  $\text{Ni}^{2+}$ ,  $\text{Rh}^{3+}$ ,  $\text{Pd}^{2+}$ ) may be trapped in low-lying MC states. Accordingly, the alteration of the emissive properties is not specific to the  $\text{Pd}^{2+}$  cation.

## Conclusion

From the present detailed theoretical investigation of the structural, bonding, optical and emissive properties of a series of **1-M** complexes generated by the complexation of various  $[M(Cl)_x(H_2O)_n]^q$  compounds ( $M = Ca^{2+}, Mn^{2+}, Fe^{2+}, Co^{2+}, Ni^{2+}, Zn^{2+}, Rh^{3+}, Pd^{2+}, Cd^{2+}, Pt^{2+}, Au^+, Au^{3+}, Hg^{2+}, Pb^{2+}$ ;  $x=1-3$ ;  $n=0-4$ ;  $q=0,+1$ ) to  $[Ru(bpy)_2(bpym)]^{2+}$  we can conclude that this  $Ru^{2+}$  complex is not a selective probe for monitoring metal cations in water. In order to increase this selectivity design of new complexes with specific ligands and metals could be considered. Indeed, the chelation site of **1** is flexible enough for adjusting all kind of coordination sphere. Selectivity could be enhanced by the design of ligands compatible with one specific coordination sphere. For instance, large ligand could inhibit binding of cations having octahedral coordination spheres. None of the **1-M** complexes exhibit absorption spectra with low-lying absorbing  $M_MLCT$  states potentially specific to each cation if one except the **1-Fe** complex. Adapting the metal centre or the ligand of complex **1** in order to significantly increase the contribution of the chelated metal in the absorption spectrum would open new perspective in term of selectivity. Finally, the nature of the counterion, here  $Cl^-$ , could also affect drastically the optical and emissive properties of the complexes.

## Author Contributions

Dr. B. Schweitzer has performed part of the calculations. Dr. C. Gourlaouen has performed part of the calculations, of the analysis and of the writing. Dr. C. Daniel did part of the analysis and of the writing.

## Conflicts of interest

There are no conflicts to declare.

## Acknowledgements

The calculations were carried out in part at the IDRIS computer centers through a grant of computer time from GENCI (A0050810629) and in part in the Strasbourg HPC.

## Notes and references

- 1 A. Kumar, M. Chhatwal, A.K. Singh, V. Singh, M. Trivedi, *Chem. Commun.*, 2014, **50**, 8488-8490.
- 2 A. Prasanna de Silva, H. Q. Nimal Gunaratne, T. Gunnlaugsson, A. J. M. Huxley, C. P. McCoy, J. T. Rademacher, T. E. Rice, *Chem. Rev.*, 1997, **97**, 1515-1566; L. Prodi, F. Bolletta, M. Montalti, N. Zaccaroni, *Coord. Chem. Rev.*, 2000, **205**, 59-83.
- 3 V. Balzani, R. Ballardini, F. Bolletta, M. T. Gandolfi, A. Juris, M. Maestri, M. F. Manfrin, L. Moggi, N. Sabbatini, *Coord. Chem. Rev.*, 1993, **125**, 75-88.
- 4 M. H. Keefe, K. D. Benkstein; J. T. Hupp, *Coord. Chem. Rev.*, 2000, **205**, 201; S.-S. Sun, A. J. Lees, *Coord. Chem. Rev.*, 2002, **230**, 171-192.
- 5 C. W. Rogers, M. O. Wolf, *Coord. Chem. Rev.*, 2002, **233**, 341-350.
- 6 K. K. Lo, M.-W. Louie, K. Y. Zhang, *Coord. Chem. Rev.*, 2010, **254**, 2603-2622; Q. Zhao, F. Li, C. Huang, *Chem. Soc. Rev.*, 2010, **39**, 3007-3030; V. Guerschais, J.-L. Fillaut, *Coord. Chem. Rev.*, 2011, **255**, 2448-2457; Q. Zhao, C. Huang, F. Li, *Chem. Soc. Rev.*, 2011, **40**, 2508-2524; Z. Liu, W. He, Z. Guo, *Chem. Soc. Rev.*, 2013, **42**, 1568-1600.
- 7 H. Q. Yin, X. B. Yin, *Acc. Chem. Res.* 2020, **53**, 485; S. A. A. Razavi, A. Morsali, *Coord. Chem. Rev.*, 2020, **415**, 213299; S. M. Kanan, A. Malkawi, *Comments Inorg. Chem.*, 2021, **41**, 1-66.
- 8 Q. Xiao, D. Liu, Y. Wei, G. A. Cui, *Polyhedron*, 2019, **158**, 342-351; J. Jin, C. Jiang, W. Chang, G. Xu, X. Fu, *Inorg. Chem. Commun.*, 2016, **70**, 157-159; L. Qian, Z. Wang, J. Ding, H. Tian, K. Li, B. Li, H. Li, *Dyes Pigm.*, 2020, **175**, 108159; X. Tian, S. Yao, C. Qiu, T. Zheng, Y. Chen, H. Huang, J. Chen, S. Liu, H. Wen, *Inorg. Chem.*, 2020, **59**, 2803-2810; M. Besheli, R. Rahimi, Y. Farahani, V. Safarifard, *Inorg. Chim. Acta.*, 2019, **495**, 118956; K. Fan, S. Bao, W. Nie, C. Liao, L. Zheng, *Inorg. Chem.*, 2018, **57**, 1079-1089.
- 9 K. K. Lo, S. P.-O. Li, *RSC Adv.*, 2014, **4**, 10560-10585; A. K. Singh, *RSC Adv.* 2015, **5**, 30187-30191; A. K. Singh, R. Nagarajan, *Dalton Trans.*, 2015, **44**, 19786-19790; A. K. Singh, G. Pandey, K. Singh, A. Kumar, M. Trivedi, V. Singh, *Dalton Trans.*, 2018, **47**, 6386-6393; T.-S. Kang, J.-T. Zhang, K. Vellaisamy, D.-L. Ma, C.-H. Leung, *Dalton Trans.*, 2018, **47**, 13314-13317; R. Pandey, A. Kumar, Q. Xu, D. S. Pandey, *Dalton Trans.*, 2020, **49**, 542-568; L.-J. Han, Y.-J. Kong, Y.-Y. Xu, M.-M. Huang, *Polyhedron*, 2021, **193**, 114868.
- 10 C. Sousa, M. Alias, A. Domingo, C. de Graaf, *Chem. Eur. J.*, 2019, **25**, 1152; S. Mai, F. Plasser, J. Dorn, M. Fumanal, C. Daniel, L. Gonzalez, *Coord. Chem. Rev.*, 2018, **361**, 74-97; C. Daniel, *Phys. Chem. Chem. Phys.*, 2021, **23**, 43-58; T. Hosseinejad, F. Ebrahimpour-Malmir, B. Fattahi, *RSC Adv.*, 2018, **8**, 12232-12259; J. Zheng, H. Yang, M. Xie, D. Li, *Chem. Commun.*, 2019, **55**, 7134-7146; H. Lischka, D. Nachtigallová, A. J. A. Aquino, P. G. Szalay, F. Plasser, F. B. C. Machado, M. Barbatti, *Chem. Rev.*, 2018, **118**, 7293-7361; P. Li, K. M. Jr Merz, *Chem. Rev.*, 2017, **117**, 1564-1686.
- 11 A. Wang, R. Fan, Y. Zhou, X. Zheng, X. Zhou, S. Hao, Y. Yang, *Coord. Chem.*, 2019, **72**, 102-118; M. A. Treto-Suárez, Y. Hidalgo-Rosa, E. Schott, X. Zarate, D. Pérez-Hernández, *Int. J. Quant. Chem.*, 2020, **120**, e26083.
- 12 D. D. Wang, Q.-M. Zhu, S. Li, J.-Y. Guo, H.-Y. Shen, X.-R. Wang, W.-X. Chai, *Polyhedron*, 2020, **175**, 114178; M. A. Muddassar, *J. Organomet. Chem.*, 2020, **926**, 121499.
- 13 Gaussian 09, Revision D.01, Frisch, M. J.; Trucks, G. W.; Schlegel, H. B.; Scuseria, G. E.; Robb, M. A.; Cheeseman, J. R.; Scalmani, G.; Barone, V.; Petersson, G. A.; Nakatsuji, H.; Li, X.; Caricato, M.; Marenich, A. V.; Bloino, J.; Janesko, B. G.; Gomperts, R.; Mennucci, B.; Hratchian, H. P.; Ortiz, J. V.; Izmaylov, A. F.; Sonnenberg, J. L.; Williams-Young, D.; Ding, F.; Lipparini, F.; Egidi, F.; Goings, J.; Peng, B.; Petrone, A.; Henderson, T.; Ranasinghe, D.; Zakrzewski, V. G.; Gao, J.; Rega, N.; Zheng, G.; Liang, W.; Hada, M.; Ehara, M.; Toyota, K.; Fukuda, R.; Hasegawa, J.; Ishida, M.; Nakajima, T.; Honda, Y.; Kitao, O.; Nakai, H.; Vreven, T.; Throssell, K.; Montgomery, J. A., Jr.; Peralta, J. E.; Ogliaro, F.; Bearpark, M. J.; Heyd, J. J.; Brothers, E. N.; Kudin, K. N.; Staroverov, V. N.; Keith, T. A.; Kobayashi, R.; Normand, J.; Raghavachari, K.; Rendell, A. P.; Burant, J. C.; Iyengar, S. S.; Tomasi, J.; Cossi, M.; Millam, J. M.; Klene, M.; Adamo, C.; Cammi, R.; Ochterski, J. W.; Martin, R. L.; Morokuma, K.; Farkas, O.; Foresman, J. B.; Fox, D. J. Gaussian 09 (Gaussian, Inc., Wallingford CT, 2009).
- 14 S. Grimme, J. Antony, S. Ehllich, H. Krieg, *J. Chem. Phys.*, 2010, **132**, 154104.
- 15 R. Ditchfield, W. J. Hehre, J. A. Pople, *J. Chem. Phys.*, 1971, **54**, 724-728.

- 16 P. Fuentealba, H. Preuss, H. Stoll, L. Szentpály, *Chem. Phys. Lett.*, 1982, **89**, 418-422.
- 17 S. Miertuš, E. Scrocco, J. Tomasi, *Chem. Phys.*, 1981, **55**, 117
- 18 ADF 2019.3, SCM, Theoretical Chemistry, Vrije Universiteit, Amsterdam, The Netherlands, <http://www.scm.com>
- 19 E. van Lenthe, E. J. Baerends, *J. Comp. Chem.*, 2003, **24**, 1142-1156.
- 20 E. van Lenthe, A. E. Ehlers, E. J. Baerends, *J. Chem. Phys.*, 1999, **110**, 8943-8953.
- 21 C. C. Pye, T. A. Ziegler, *Theor. Chem. Acc.*, 1999, **101**, 396-408.
- 22 E. K. U. Gross, J. F. Dobson M. Petersilka, in *Density Functional Theory*, R.F. Nalewajski, Editor. 1996, Springer: Heidelberg.
- 23 F. Wang, T. A. Ziegler, *J. Chem. Phys.*, 2005, **123**, 154102.
- 24 S. Hirata, M. Head-Gordon, *Chem. Phys. Lett.*, 1999, **314**, 291-299.
- 25 F. Plasser *J. Chem. Phys.* 2020, **152**, 084108.
- 26 L. Shimoni-Livny, J. P. Glusker, C. W. Bock, *Inorg. Chem.*, 1998, **37**, 1853-1867.

## Electronic Supplementary Informations

Are luminescent Ru<sup>2+</sup> chelated complexes selective coordinative sensors for the detection of heavy cations ?

C. Gourlaouen, B. Schweitzer and C. Daniel

Figure S1 : spectra of <b>1</b> , in black without SOC, in red with SOC	3
Figure S2: spectra of <b>1-Ca</b>	3
Figure S3: spectra of <b>1-Mn</b>	4
Figure S4: spectra of <b>1-Fe</b>	4
Figure S5 : spectra of <b>1-Co</b>	5
Figure S6: spectra of <b>1-Ni</b>	5
Figure S7: spectra of <b>1-Zn</b>	6
Figure S8: spectra of <b>1-Rh</b>	6
Figure S9: spectra of <b>1-Pd</b> , in black without SOC and in red with SOC	7
Figure S10: spectra of <b>1-Cd</b>	7
Figure S11: spectra of <b>1-Pt</b> , in black without SOC and in red with SOC	8
Figure S12: spectra of <b>1-Au(I)</b>	8
Figure S13: spectra of <b>1-Au(III)</b>	9
Figure S14: spectra of <b>1-Hg</b>	9
Figure S15: spectra of <b>1-Pb</b>	10
Figure S16: Character of the low-lying triplet states (T <sub>1</sub> -T <sub>15</sub> ) of <b>1</b>	10
Figure S17: Character of the low-lying triplet states (T <sub>1</sub> -T <sub>30</sub> ) of <b>1-Pd</b>	10
Figure S18: : Character of the low-lying singlet states of <b>1-Fe</b>	10
Figure S19: Character of the low-lying singlet states of <b>1-Rh</b> .	11
Figure S20 : Character of the low-lying singlet states of <b>1-Au(I)</b>	11
Figure S21 : Character of the low-lying singlet states of <b>1-Au(III)</b>	11
Figure S22 : Character of the low-lying singlet states of <b>1-Hg</b>	11
Table S1: Energy (in Ev), oscillator strength and nature of the singlet states of <b>1</b>	12
Table S2: Energy (in Ev), oscillator strength and nature of the singlet states of <b>1-Ca</b>	12
Table S3: Energy (in Ev), oscillator strength and nature of the singlet states of <b>1-Mn</b>	13
Table S4: Energy (in Ev), oscillator strength and nature of the singlet states of <b>1-Fe</b>	15
Table S5: Energy (in Ev), oscillator strength and nature of the singlet states of <b>1-Co</b>	16
Table S6: Energy (in Ev), oscillator strength and nature of the singlet states of <b>1-Ni</b>	18
Table S7: Energy (in Ev), oscillator strength and nature of the singlet states of <b>1-Zn</b>	19
Table S8: Energy (in Ev), oscillator strength and nature of the singlet states of <b>1-Rh</b>	20
Table S9: Energy (in Ev), oscillator strength and nature of the singlet states of <b>1-Pd</b>	21
Table S10: Energy (in Ev), oscillator strength and nature of the singlet states of <b>1-Cd</b>	22
Table S11: Energy (in Ev), oscillator strength and nature of the singlet states of <b>1-Pt</b>	23
Table S12: Energy (in Ev), oscillator strength and nature of the singlet states of <b>1-Au(I)</b>	24
Table S13: Energy (in Ev), oscillator strength and nature of the singlet states of <b>1-Au(III)</b>	25
Table S14: Energy (in Ev), oscillator strength and nature of the singlet states of <b>1-Hg</b>	26
Table S15: Energy (in Ev), oscillator strength and nature of the singlet states of <b>1-Pb</b>	27

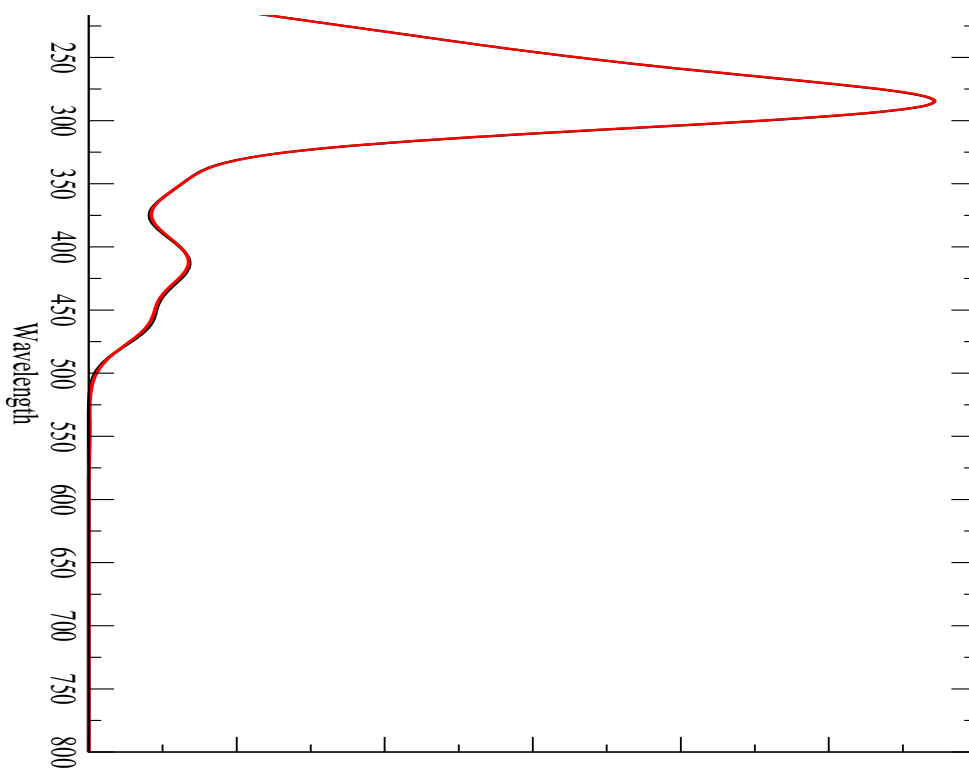


Figure S1 : spectra of **1**, in black without SOC, in red with SOC

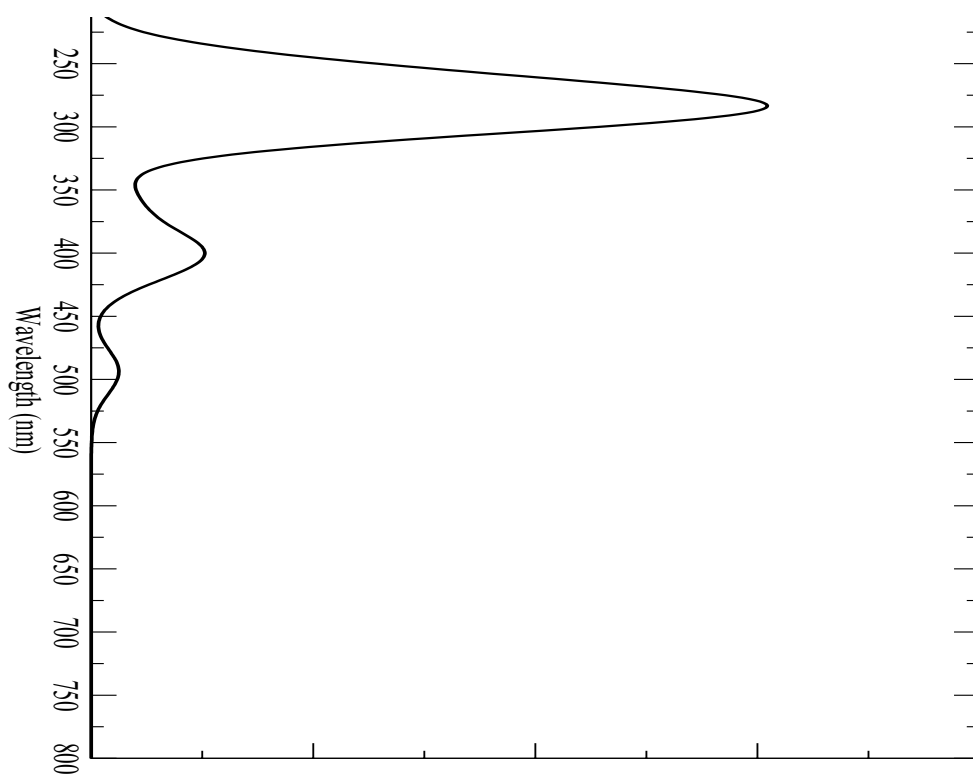


Figure S2: spectra of **1-Ca**

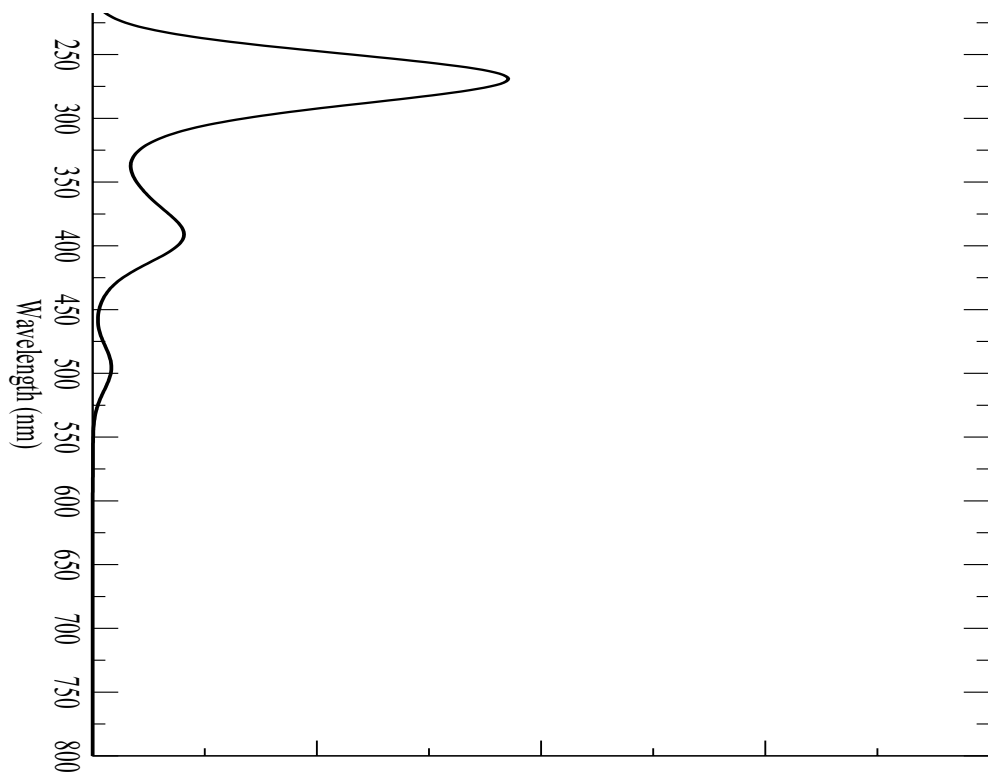


Figure S3: spectra of **1-Mn**

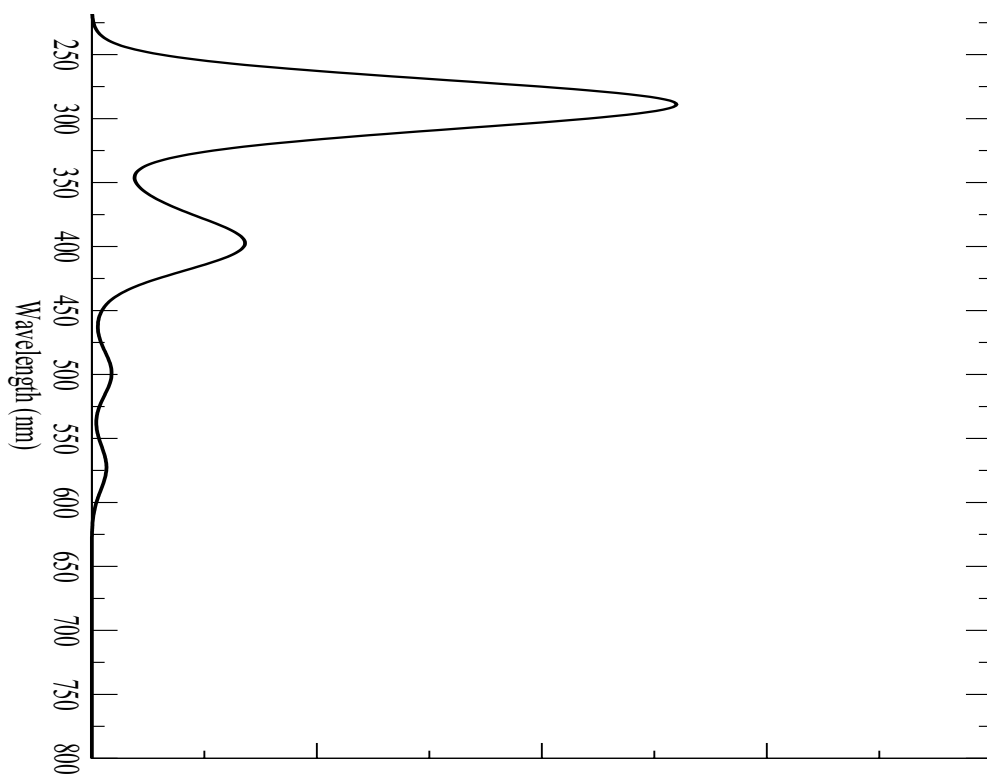


Figure S4: spectra of **1-Fe**

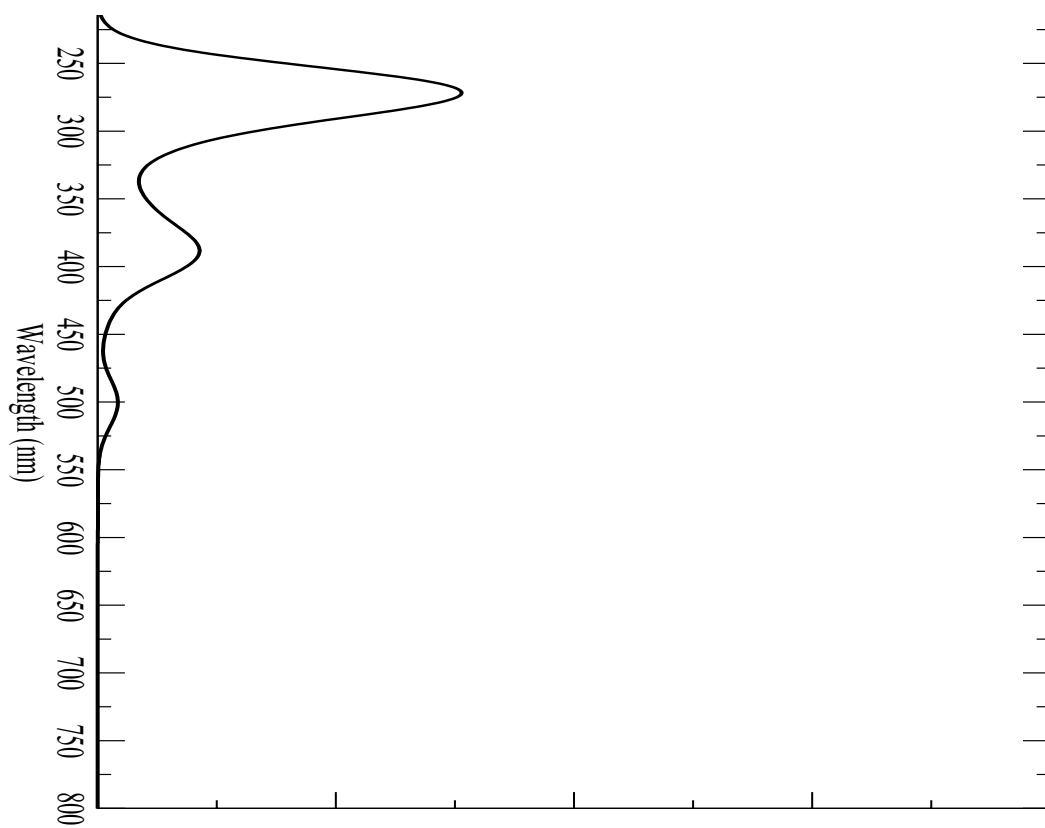


Figure S5 : spectra of **1-Co**

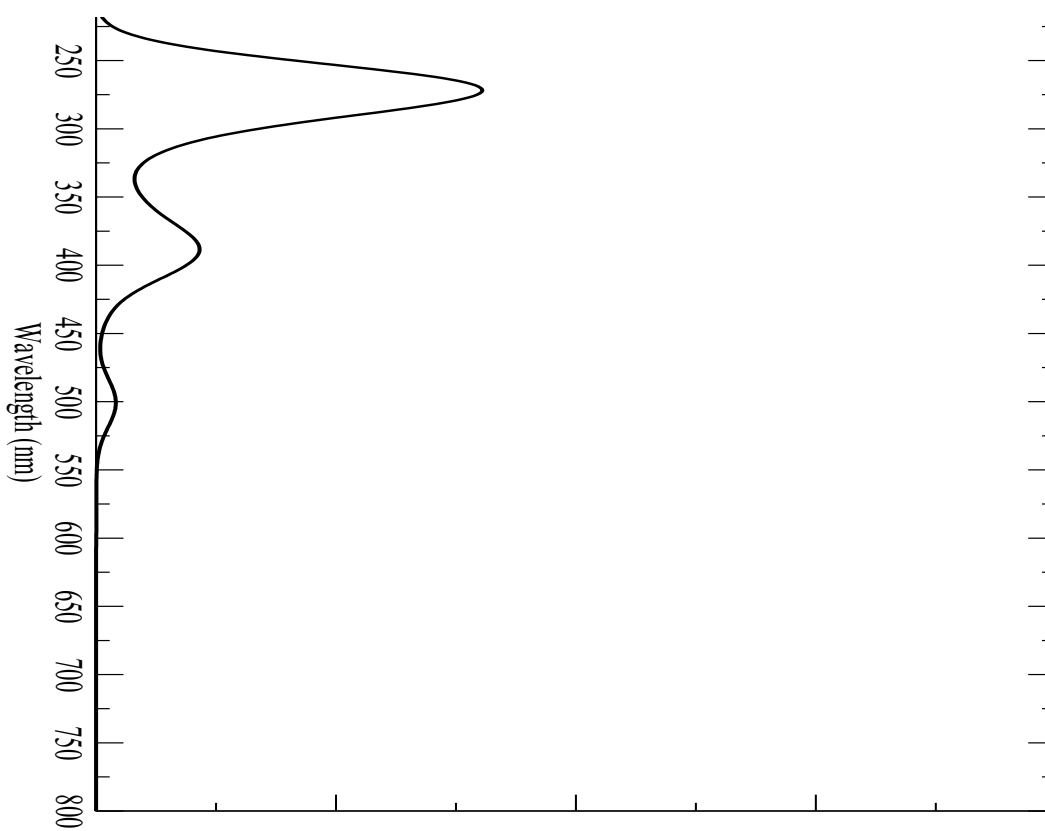


Figure S6: spectra of **1-Ni**



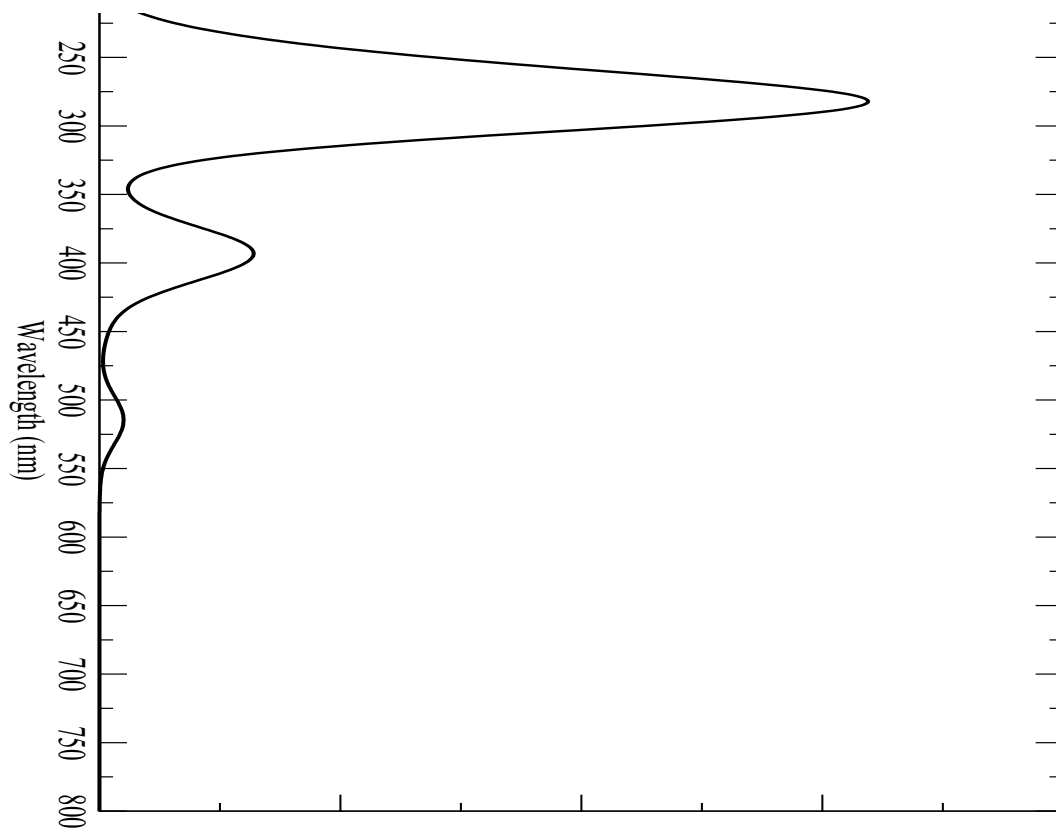


Figure S7: spectra of **1-Zn**

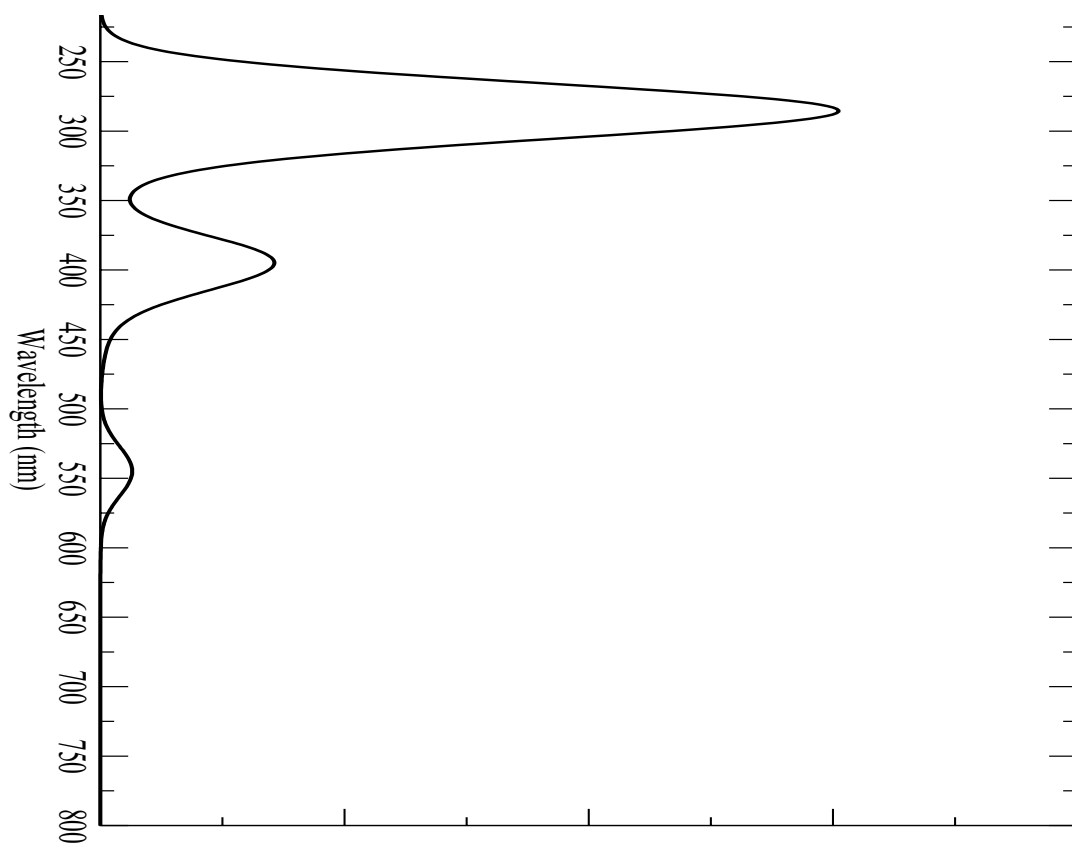


Figure S8: spectra of **1-Rh**

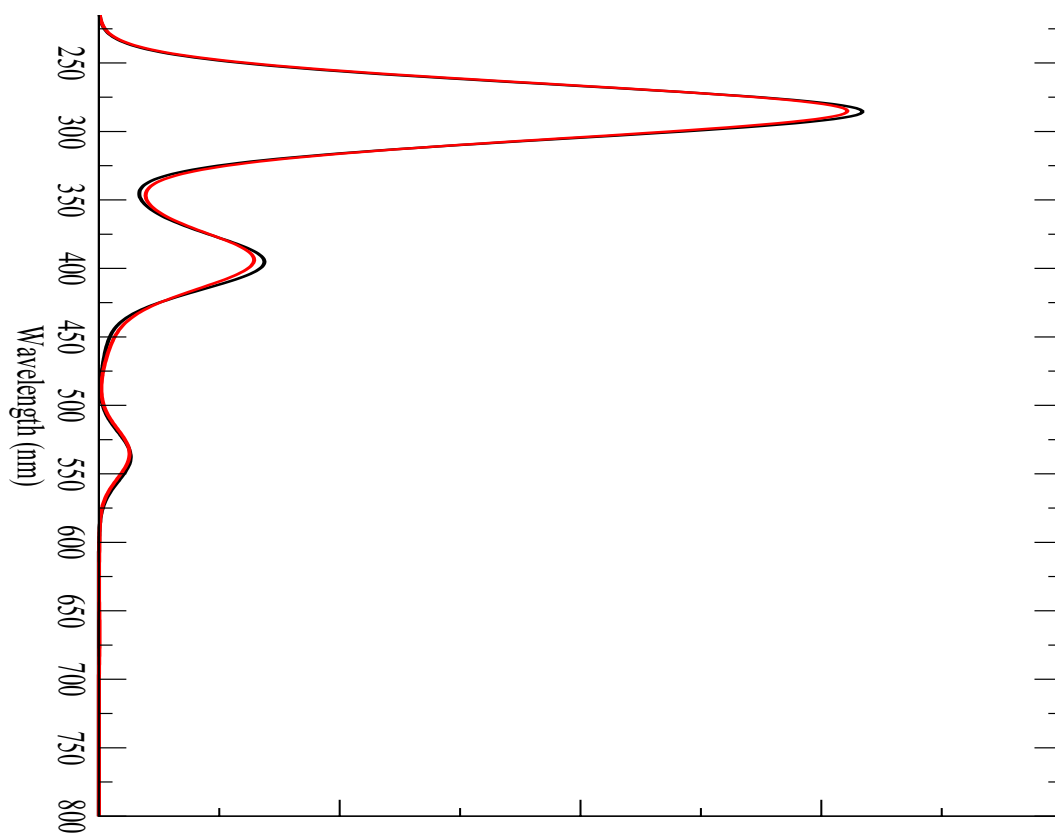


Figure S9: spectra of **1-Pd**, in black without SOC and in red with SOC

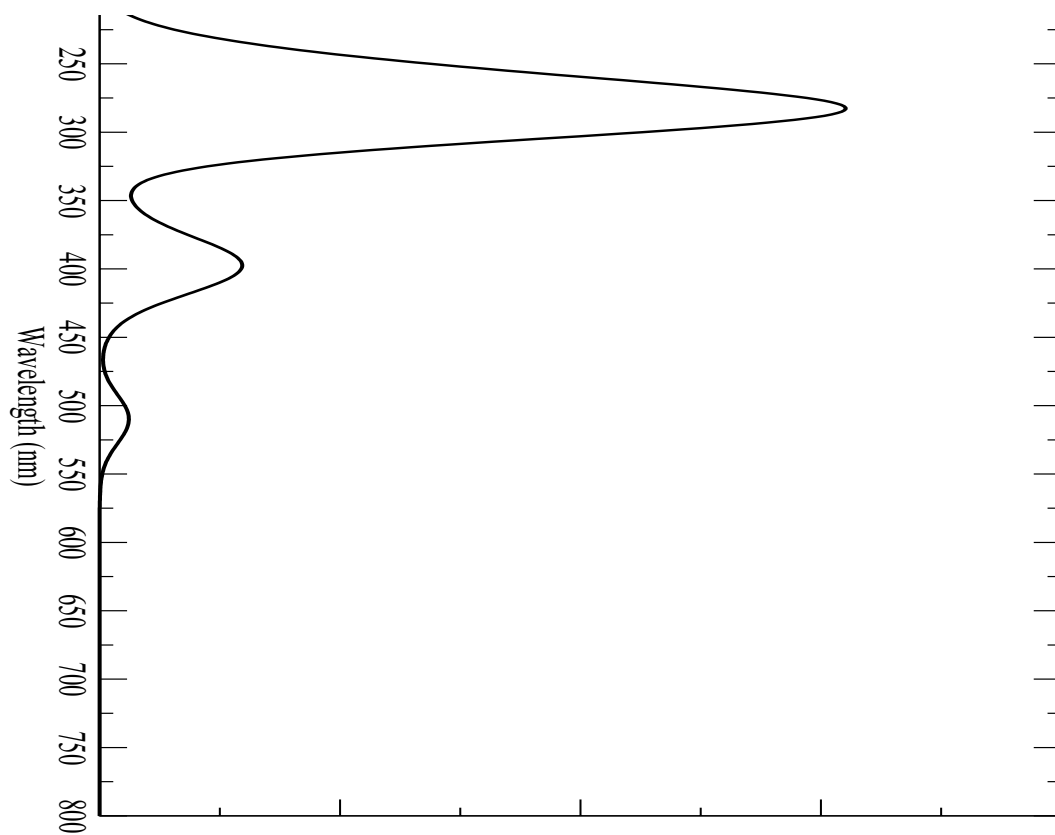


Figure S10: spectra of **1-Cd**

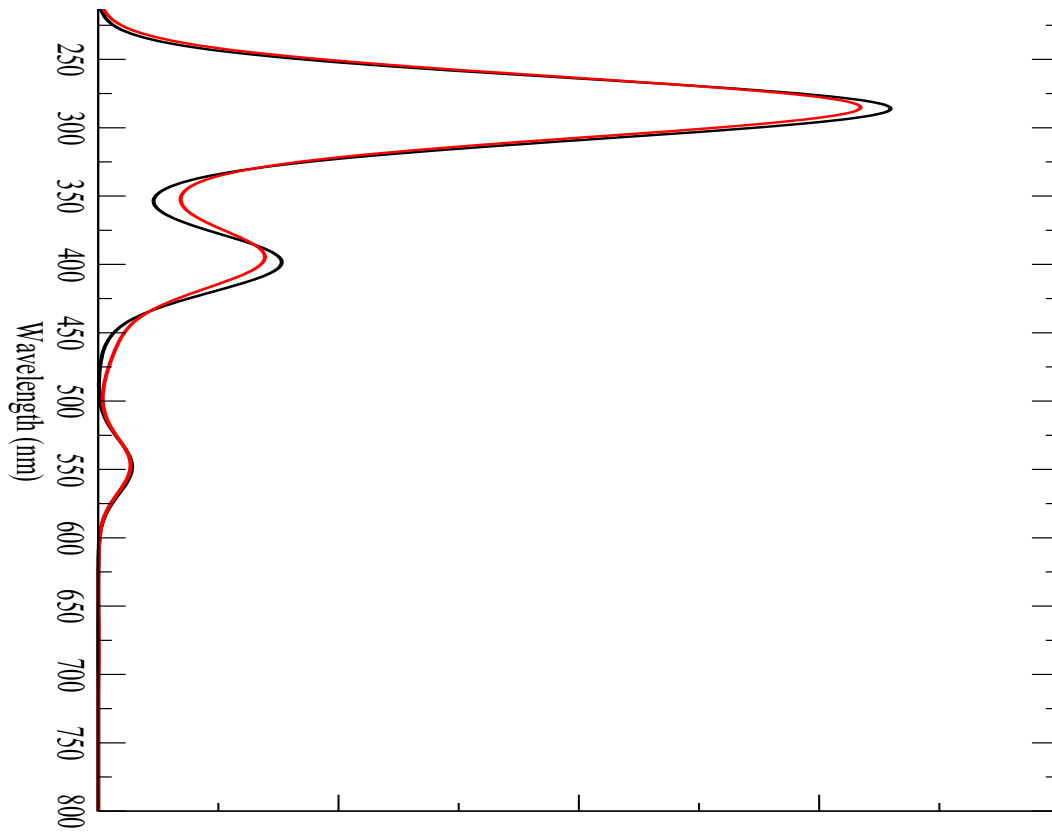


Figure S11: spectra of **1-Pt**, in black without SOC and in red with SOC

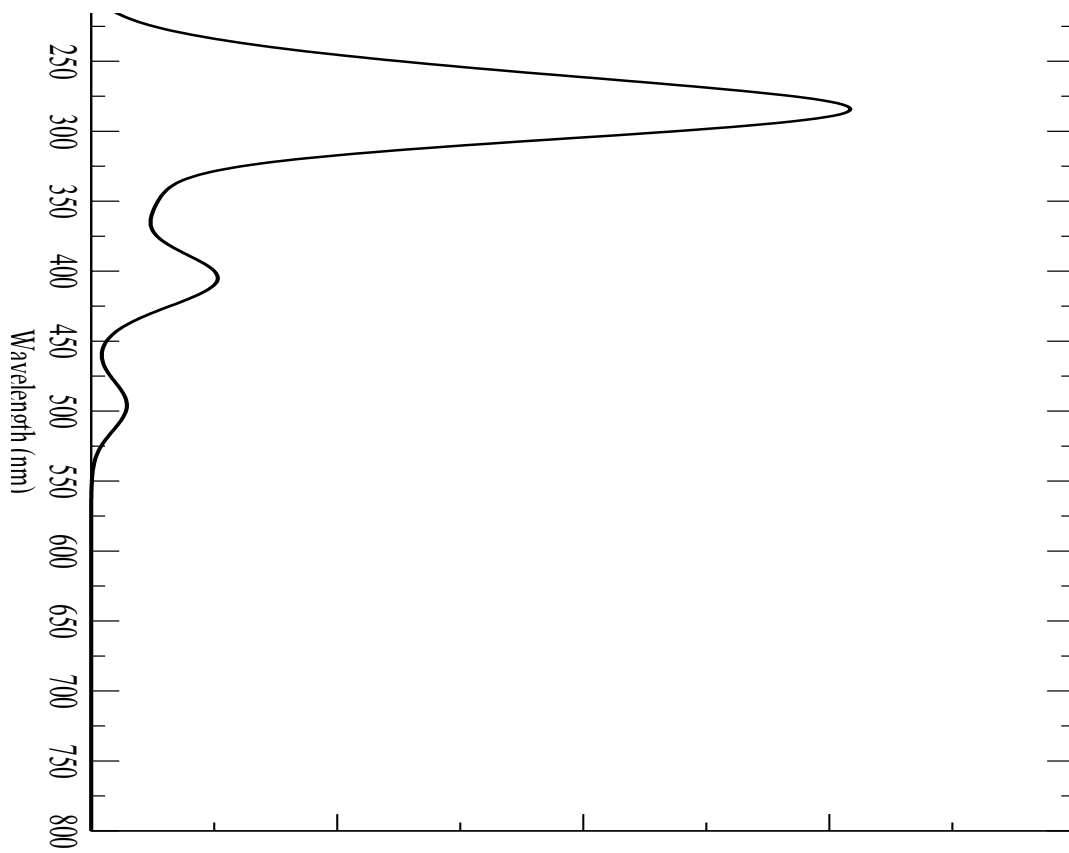


Figure S12: spectra of **1-Au(I)**

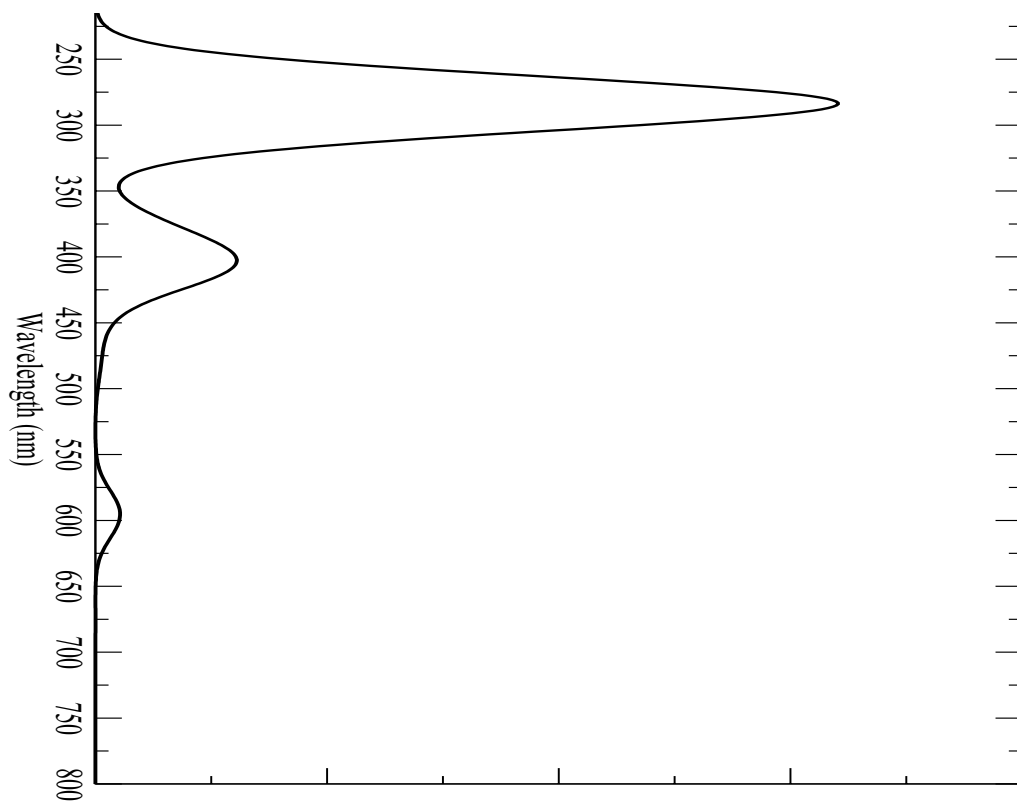


Figure S13: spectra of **1-Au(III)**

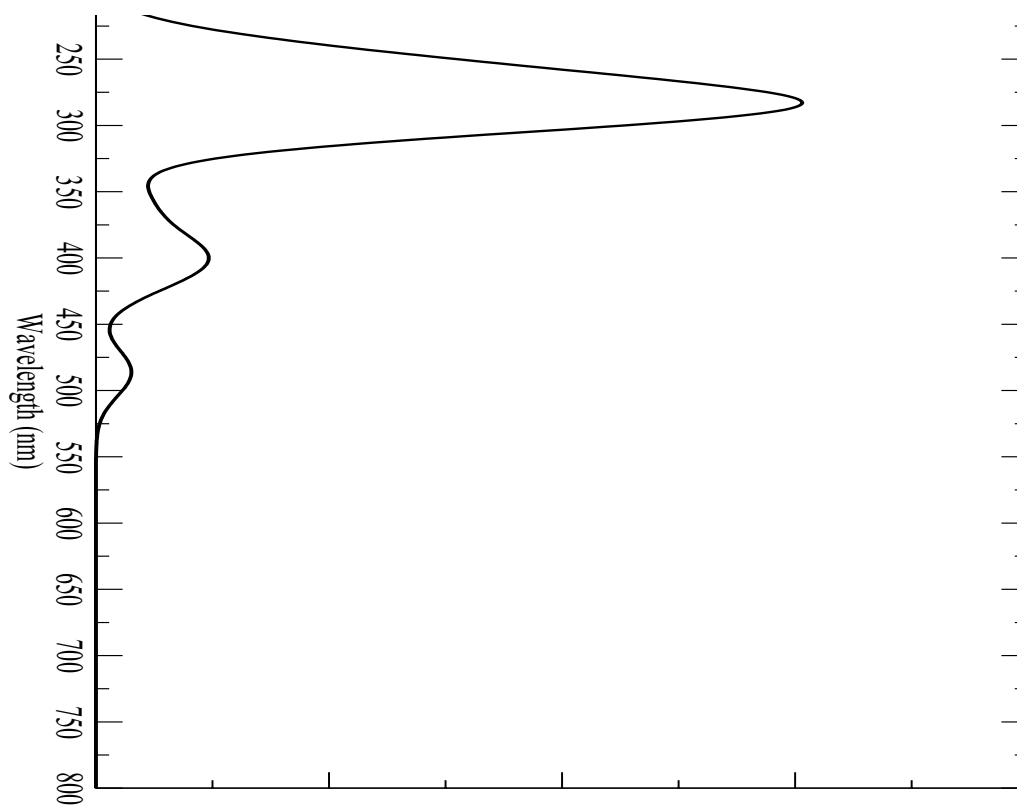
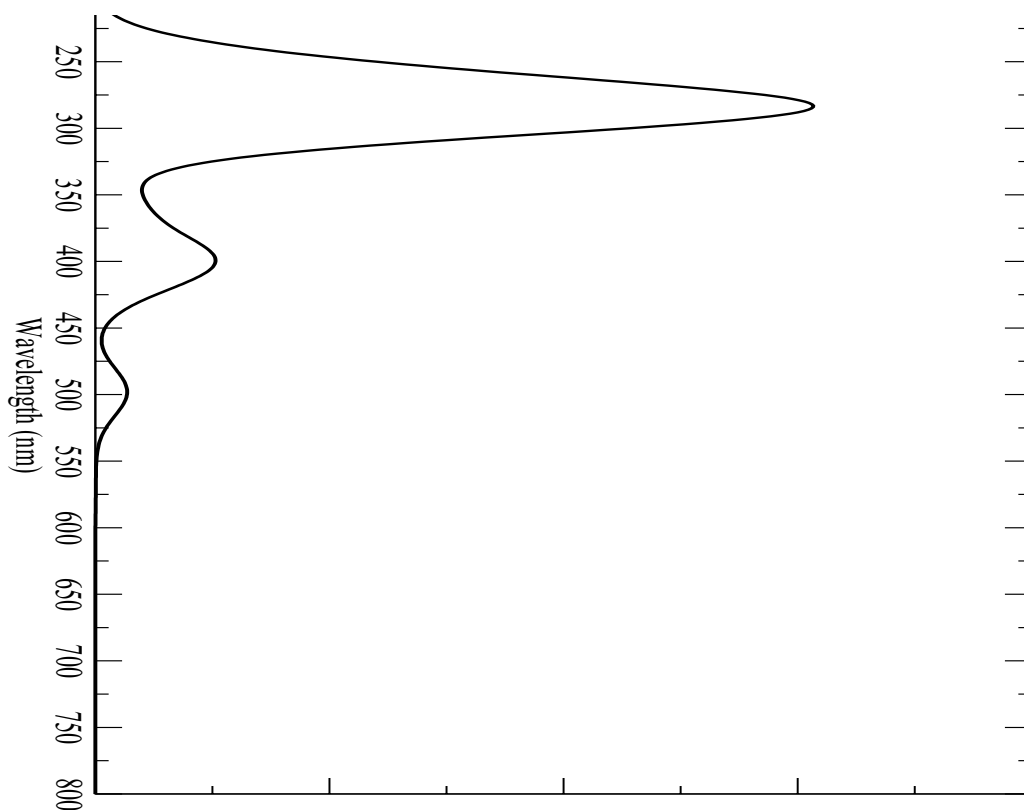
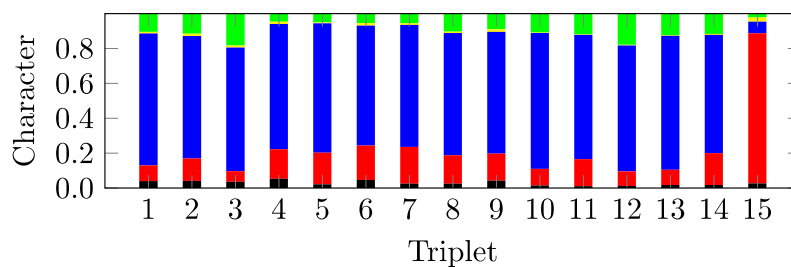
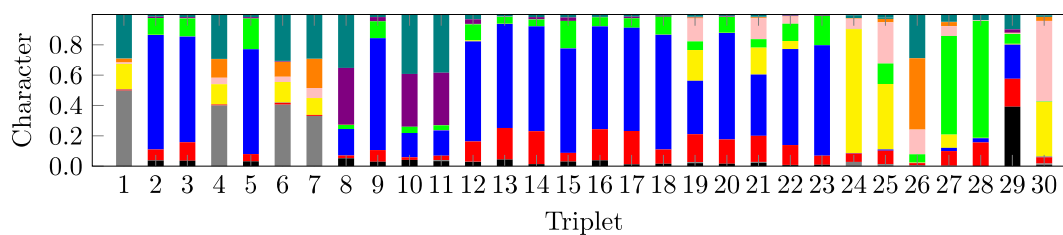
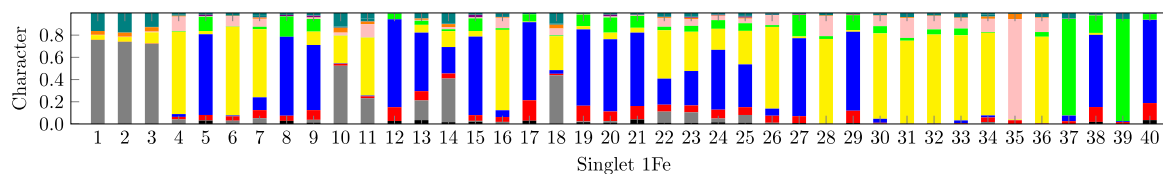


Figure S14: spectra of **1-Hg**

Figure S15: spectra of **1-Pb**Figure S16: Character of the low-lying triplet states ( $T_1$ - $T_{13}$ ) of **1**Figure S17: Character of the low-lying triplet states ( $T_1$ - $T_{30}$ ) of **1-Pd**Figure S18: : Character of the low-lying singlet states of **1-Fe**

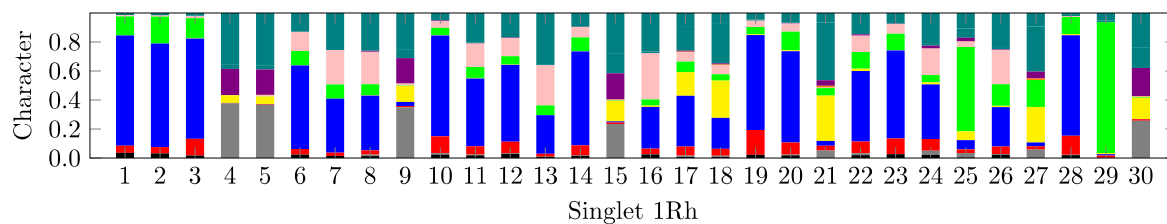


Figure S19: Character of the low-lying singlet states of **1-Rh**.

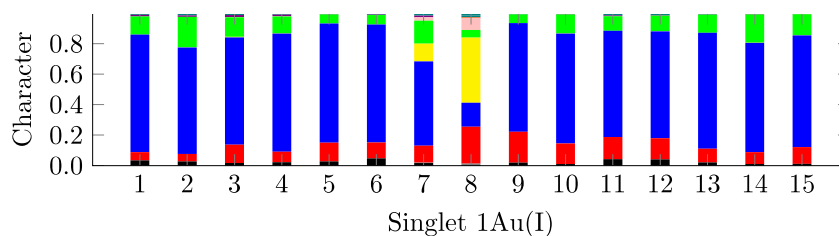


Figure S20: Character of the low-lying singlet states of **1-Au(I)**

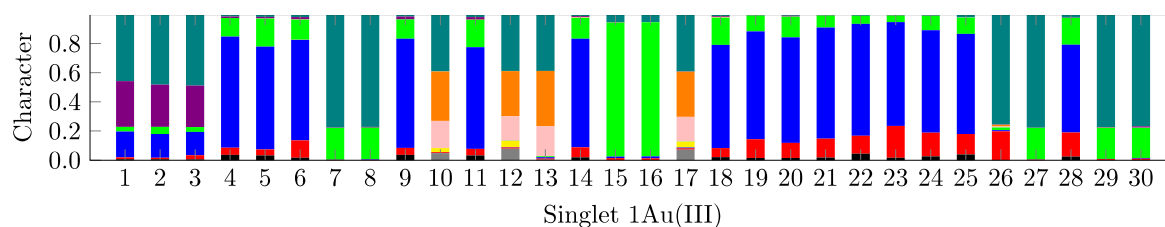


Figure S21: Character of the low-lying singlet states of **1-Au(III)**

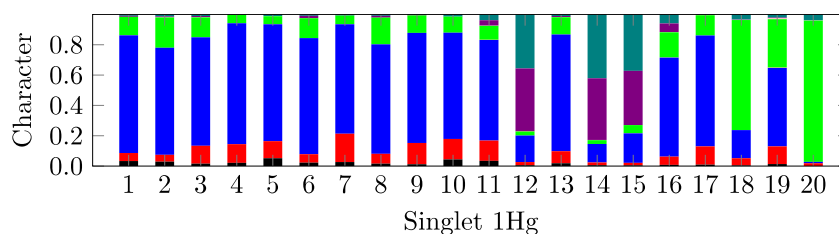


Figure S22: Character of the low-lying singlet states of **1-Hg**

The color code for figures S16 and S17: blue for  $M_{Ru}LCT$ ; green for  $LLCT$ ; red for  $LC$ ; black and grey for  $MC$  (Ru or Pd); pink for  $XLCT$ ; yellow for  $M_{Pd}LCT$ ; orange for  $XM_{Pd}CT$ ; violet for  $M_{Ru}M_{Pd}CT$ ; teal for other transitions.

Table S1: Energy (in Ev), oscillator strength and nature of the singlet states of 1

State	Energy	Oscillator	M <sub>0</sub> C	LC	M <sub>0</sub> LCT	LLCT	Other
1	2.391	0.00E+00	3.27%	5.75%	78.43%	11.85%	0.70%
2	2.550	3.00E-03	2.79%	5.19%	71.81%	19.30%	0.91%
3	2.686	1.76E-01	1.62%	12.24%	72.90%	12.66%	0.58%
4	2.733	3.00E-03	2.29%	11.96%	79.23%	6.03%	0.50%
5	2.765	5.00E-03	5.09%	11.24%	76.66%	5.91%	1.10%
6	2.880	7.50E-02	2.74%	18.21%	72.24%	5.93%	0.87%
7	2.940	3.00E-03	2.93%	14.73%	71.39%	9.98%	0.97%
8	2.979	2.01E-01	4.19%	14.51%	70.48%	9.50%	1.33%
9	3.104	3.40E-02	1.48%	6.74%	78.88%	12.56%	0.34%
10	3.164	1.18E-01	2.36%	16.20%	72.28%	8.28%	0.88%
11	3.252	1.10E-02	1.40%	6.80%	72.12%	19.21%	0.47%
12	3.318	3.00E-03	1.65%	9.05%	76.47%	12.34%	0.49%
13	3.451	0.00E+00	1.02%	6.88%	73.98%	17.72%	0.39%
14	3.540	1.04E-01	0.99%	11.97%	73.47%	13.23%	0.35%
15	3.567	1.41E-01	1.01%	10.66%	74.68%	13.13%	0.53%
16	3.664	4.00E-03	1.39%	14.00%	77.63%	6.61%	0.37%
17	3.816	4.80E-02	1.71%	19.53%	72.17%	6.11%	0.49%
18	3.838	1.00E-03	2.46%	13.96%	75.66%	7.35%	0.57%
19	3.875	3.30E-02	2.46%	17.07%	69.33%	10.40%	0.75%
20	3.904	1.00E-03	0.05%	3.99%	3.24%	89.90%	2.82%
21	3.943	4.00E-03	13.30%	12.43%	65.71%	5.87%	2.69%
22	3.950	1.20E-02	0.69%	4.82%	2.43%	89.28%	2.78%
23	3.956	4.00E-03	43.71%	5.59%	37.44%	4.53%	8.73%
24	3.964	6.40E-02	6.12%	11.44%	75.20%	5.97%	1.28%
25	3.973	0.00E+00	40.51%	6.66%	40.72%	3.92%	8.20%
26	4.003	4.00E-03	0.92%	22.01%	70.75%	5.79%	0.53%
27	4.010	1.12E-01	4.01%	16.26%	66.25%	12.13%	1.35%
28	4.072	2.00E-02	11.21%	11.48%	64.59%	9.73%	2.99%
29	4.087	1.00E-03	36.54%	8.06%	41.10%	4.88%	9.41%
30	4.102	1.60E-02	8.04%	27.97%	56.32%	4.94%	2.74%
31	4.104	7.00E-03	1.40%	25.28%	62.77%	9.53%	1.03%
32	4.161	1.00E-03	0.06%	90.90%	2.05%	4.16%	2.84%
33	4.234	2.83E-01	0.51%	81.80%	11.74%	3.71%	2.23%
34	4.279	4.57E-01	0.18%	87.51%	6.35%	3.37%	2.58%
35	4.302	1.29E+00	0.53%	81.95%	10.66%	1.97%	4.89%
36	4.332	2.86E-01	0.24%	86.41%	6.04%	2.10%	5.22%
37	4.475	2.20E-02	5.69%	15.50%	61.25%	14.40%	3.17%
38	4.543	1.70E-02	2.95%	11.68%	4.88%	77.39%	3.10%
39	4.562	7.00E-03	18.27%	56.68%	11.84%	6.80%	6.41%
40	4.566	1.00E-03	46.67%	5.95%	29.20%	6.31%	11.86%
41	4.581	2.80E-02	1.82%	21.34%	1.76%	72.23%	2.84%
42	4.591	1.00E-02	29.04%	29.48%	18.43%	14.74%	8.30%
43	4.697	0.00E+00	44.83%	6.69%	30.51%	4.75%	13.22%
44	4.760	1.01E+00	0.09%	87.34%	1.55%	8.02%	2.99%
45	4.798	0.00E+00	0.21%	88.52%	2.48%	6.66%	2.13%
46	4.800	6.00E-03	0.01%	3.74%	0.38%	94.66%	1.22%
47	4.846	4.00E-03	0.02%	3.27%	1.00%	94.51%	1.20%
48	4.927	1.60E-02	0.06%	92.96%	1.72%	3.75%	1.51%
49	4.986	4.00E-03	1.57%	8.46%	73.22%	15.88%	0.86%
50	5.020	6.20E-02	0.03%	8.85%	0.67%	87.70%	2.75%
51	5.050	1.10E-02	0.18%	72.63%	8.75%	17.22%	1.23%
52	5.057	1.00E-03	0.87%	32.00%	53.38%	13.07%	0.68%
53	5.063	1.10E-02	0.12%	18.42%	3.18%	75.59%	2.70%
54	5.076	2.50E-02	0.88%	9.47%	45.59%	41.97%	2.09%
55	5.096	1.60E-02	0.57%	13.72%	20.11%	61.82%	3.78%
56	5.107	5.80E-02	0.01%	83.05%	3.69%	11.80%	1.44%
57	5.128	2.00E-03	0.14%	17.67%	2.79%	74.43%	4.97%
58	5.202	4.30E-02	0.12%	65.80%	22.25%	10.71%	1.12%
59	5.203	0.00E+00	1.19%	51.35%	38.94%	7.27%	1.25%
60	5.227	9.00E-03	0.49%	56.33%	19.54%	21.76%	1.88%
61	5.258	4.20E-02	0.03%	90.26%	4.46%	2.92%	2.34%
62	5.259	0.00E+00	0.05%	23.08%	1.49%	72.94%	2.44%
63	5.279	3.00E-03	0.67%	39.88%	30.67%	27.47%	1.31%
64	5.297	0.00E+00	0.22%	68.34%	14.98%	14.26%	2.21%
65	5.325	2.30E-02	0.29%	32.54%	15.47%	49.19%	2.52%
66	5.333	7.90E-02	0.06%	15.17%	4.01%	78.18%	2.58%
67	5.341	3.60E-02	0.29%	30.02%	57.70%	11.31%	0.69%
68	5.374	2.80E-02	0.76%	37.39%	51.91%	8.65%	1.30%
69	5.395	2.80E-02	0.68%	32.40%	53.67%	12.48%	0.77%
70	5.400	1.00E-03	0.02%	96.15%	1.10%	1.58%	1.15%
71	5.429	2.50E-02	0.11%	78.97%	12.92%	6.96%	1.04%
72	5.452	5.40E-02	0.11%	15.44%	5.91%	75.73%	2.81%
73	5.459	2.00E-03	0.16%	24.18%	31.14%	43.31%	1.21%
74	5.469	7.00E-03	0.15%	21.21%	36.18%	41.48%	0.99%
75	5.485	1.12E-01	0.23%	41.77%	17.80%	38.29%	1.90%
76	5.500	0.00E+00	2.37%	19.58%	49.67%	27.11%	1.27%
77	5.530	2.00E-03	10.75%	14.87%	18.87%	49.73%	5.78%
78	5.542	0.00E+00	15.46%	10.35%	29.70%	38.35%	6.15%
79	5.544	3.00E-03	0.23%	82.15%	1.86%	12.66%	3.10%
80	5.575	1.38E-01	0.85%	35.60%	7.86%	52.91%	2.78%

Table S2: Energy (in Ev), oscillator strength and nature of the singlet states of 1-Ca

State	Energy	Oscillator	M <sub>0</sub> C	M <sub>0</sub> C	LC	M <sub>0</sub> LCT	M <sub>0</sub> LCT	LLCT	XLCT	XMCT	M <sub>0</sub> M <sub>0</sub> CT	M <sub>0</sub> M <sub>0</sub> CT	Other
1	2.170	0.00E+00	3.36%	0.00%	5.37%	77.67%	0.03%	12.26%	0.01%	0.00%	0.36%	0.00%	0.95%
2	2.335	2.00E-03	2.83%	0.00%	4.92%	71.57%	0.02%	19.08%	0.01%	0.00%	0.39%	0.00%	1.19%
3	2.503	1.24E-01	1.53%	0.00%	11.56%	71.55%	0.01%	13.76%	0.05%	0.01%	0.53%	0.00%	1.00%
4	2.823	4.00E-03	2.80%	0.00%	12.39%	78.83%	0.02%	5.35%	0.01%	0.00%	0.01%	0.00%	0.60%
5	2.843	3.00E-03	5.02%	0.00%	11.36%	77.15%	0.02%	5.40%	0.01%	0.00%	0.01%	0.00%	1.04%





14	2.838	9.29E-04											
15	2.860	1.15E-03											
16	2.872	4.21E-05											
17	2.879	1.19E-02											
18	2.934	4.18E-04											
19	2.938	4.13E-04											
20	2.956	7.96E-04											
21	2.991	1.63E-02											
22	3.020	1.56E-02											
23	3.025	4.71E-03											
24	3.083	7.63E-03											
25	3.101	1.71E-03											
26	3.117	1.77E-02											
27	3.127	1.73E-01											
28	3.151	1.04E-01											
29	3.196	5.07E-04											
30	3.228	7.68E-04											
31	3.275	5.48E-02											
32	3.325	3.83E-03											
33	3.358	6.56E-02											
34	3.372	5.34E-03											
35	3.373	1.70E-02											
36	3.396	2.17E-03											
37	3.434	8.36E-04											
38	3.458	9.05E-06											
39	3.492	6.98E-03											
40	3.524	6.53E-04											
41	3.535	2.29E-02											
42	3.535	2.01E-03											
43	3.541	1.33E-02											
44	3.565	2.99E-02											
45	3.584	8.13E-03											
46	3.589	5.59E-03											
47	3.607	2.07E-03											
48	3.612	6.96E-06											
49	3.652	8.64E-04											
50	3.677	4.84E-03											
51	3.711	7.78E-06											
52	3.738	1.41E-04											
53	3.742	2.68E-05											
54	3.747	1.66E-03											
55	3.756	4.00E-04											
56	3.761	2.10E-04											
57	3.793	1.16E-03											
58	3.853	3.02E-03											
59	3.891	1.97E-03											
60	3.901	1.50E-02											
61	3.903	4.17E-04											
62	3.913	2.85E-06											
63	3.920	1.68E-03											
64	3.923	1.31E-03											
65	3.927	1.38E-02											
66	3.932	2.23E-02											
67	3.950	2.27E-05											
68	3.953	4.11E-03											
69	3.975	6.75E-03											
70	3.978	1.55E-03											
71	3.979	9.37E-04											
72	3.984	2.80E-03											
73	3.986	1.54E-03											
74	4.013	1.53E-04											
75	4.026	4.37E-06											
76	4.039	6.68E-05											
77	4.051	3.03E-03											
78	4.065	3.91E-03											
79	4.070	8.16E-04											
80	4.087	2.19E-02											
81	4.100	1.12E-03											
82	4.123	1.93E-03											
83	4.125	8.85E-02											
84	4.142	7.87E-03											
85	4.167	3.37E-03											
86	4.174	1.26E-02											
87	4.178	1.06E-02											
88	4.182	2.91E-03											
89	4.189	2.12E-02											
90	4.214	6.32E-04											
91	4.227	1.78E-03											
92	4.235	2.52E-04											
93	4.242	2.58E-03											
94	4.255	6.53E-04											
95	4.279	5.75E-04											
96	4.280	7.35E-03											
97	4.285	5.58E-05											
98	4.289	4.02E-03											
99	4.334	3.29E-06											
100	4.337	3.00E-03											
101	4.350	2.03E-03											
102	4.383	2.14E-03											
103	4.390	6.53E-03											
104	4.420	2.11E-03											
105	4.423	3.53E-03											
106	4.439	4.29E-03											
107	4.445	5.67E-04											
108	4.459	2.08E-02											
109	4.461	1.23E-03											
110	4.469	4.44E-03											







144	4.533	1.53E-01											
145	4.540	2.33E-04											
146	4.545	6.87E-03											
147	4.551	1.10E-01											
148	4.556	2.08E-05											
149	4.567	2.78E-03											
150	4.571	6.56E-02											
151	4.591	1.61E-02											
152	4.598	6.20E-02											
153	4.609	4.59E-05											
154	4.615	9.01E-01											
155	4.632	1.10E-04											
156	4.659	1.28E-03											
157	4.674	2.43E-03											
158	4.678	2.79E-02											
159	4.714	1.20E-03											
160	4.731	7.74E-05											

Table S6: Energy (in Ev), oscillator strength and nature of the singlet states of 1-Ni

State	Energy	Oscillator	M <sub>RC</sub>	M <sub>VC</sub>	LC	M <sub>RLCT</sub>	M <sub>VLCT</sub>	LLCT	XLCT	XMCT	M <sub>RMCT</sub>	M <sub>VMCT</sub>	Other
1	1.740	9.20E-09											
2	1.768	1.50E-07											
3	1.958	2.10E-05											
4	2.035	1.44E-05											
5	2.115	6.49E-06											
6	2.123	1.75E-03											
7	2.208	4.00E-05											
8	2.279	8.72E-04											
9	2.476	8.24E-02											
10	2.521	2.82E-05											
11	2.530	7.33E-05											
12	2.564	3.43E-06											
13	2.731	2.79E-04											
14	2.732	8.82E-05											
15	2.802	4.94E-03											
16	2.802	4.31E-05											
17	2.850	6.80E-03											
18	2.857	9.92E-04											
19	2.874	2.82E-03											
20	2.885	2.80E-03											
21	2.893	1.05E-02											
22	2.953	1.22E-03											
23	2.963	2.04E-03											
24	2.978	4.86E-04											
25	3.010	1.06E-02											
26	3.026	5.86E-03											
27	3.048	3.02E-03											
28	3.051	9.79E-03											
29	3.067	4.37E-04											
30	3.110	3.71E-04											
31	3.148	1.84E-01											
32	3.155	1.15E-01											
33	3.178	1.19E-03											
34	3.221	9.98E-04											
35	3.279	7.75E-02											
36	3.338	5.55E-02											
37	3.349	2.91E-03											
38	3.363	4.48E-03											
39	3.373	2.05E-02											
40	3.395	7.92E-04											
41	3.404	2.04E-04											
42	3.442	1.55E-05											
43	3.494	3.94E-04											
44	3.496	6.65E-05											
45	3.524	5.62E-03											
46	3.534	4.22E-03											
47	3.548	4.99E-03											
48	3.558	6.43E-02											
49	3.572	3.73E-06											
50	3.587	8.46E-04											
51	3.600	6.10E-03											
52	3.608	1.33E-04											
53	3.627	2.31E-03											
54	3.669	4.11E-05											
55	3.692	5.34E-03											
56	3.702	2.97E-04											
57	3.717	7.43E-04											
58	3.743	2.74E-05											
59	3.745	1.52E-04											
60	3.758	5.25E-05											
61	3.761	1.70E-03											
62	3.765	1.43E-04											
63	3.766	2.72E-03											
64	3.785	3.27E-04											
65	3.796	9.58E-05											
66	3.814	1.06E-03											
67	3.839	2.25E-04											
68	3.872	3.01E-03											
69	3.882	2.63E-07											
70	3.917	4.21E-04											
71	3.922	1.43E-04											





















64	4.910	8.00E-03	0.73%	0.01%	3.91%	6.62%	1.18%	17.54%	63.02%	2.51%	2.11%	0.04%	2.35%
65	4.913	2.10E-02	1.40%	0.02%	6.10%	12.16%	1.39%	28.02%	41.22%	1.53%	3.93%	0.04%	4.21%
66	4.930	1.10E-02	0.02%	0.07%	4.73%	0.45%	2.13%	4.50%	81.82%	4.68%	0.11%	0.06%	1.43%
67	4.960	1.10E-02	0.26%	0.07%	19.63%	7.90%	3.93%	39.36%	21.70%	1.05%	1.80%	0.11%	4.21%
68	4.971	5.20E-02	0.26%	0.04%	12.85%	11.20%	0.41%	47.55%	13.81%	0.50%	6.61%	0.01%	6.75%
69	4.987	6.00E-03	0.14%	0.03%	6.34%	5.17%	1.96%	16.23%	64.95%	1.82%	1.15%	0.04%	2.17%
70	4.997	2.30E-02	0.90%	0.01%	7.01%	36.47%	0.15%	36.49%	0.72%	0.04%	10.85%	0.00%	7.36%
71	5.007	2.10E-02	0.73%	0.02%	13.67%	37.32%	0.91%	11.92%	16.86%	0.64%	10.82%	0.03%	7.09%
72	5.020	2.00E-03	0.03%	0.00%	7.99%	0.86%	1.03%	3.33%	82.28%	3.91%	0.12%	0.05%	0.40%
73	5.026	1.50E-02	0.05%	0.01%	34.57%	1.97%	0.66%	15.38%	43.67%	1.93%	0.22%	0.02%	1.53%
74	5.035	1.00E-02	0.03%	0.01%	31.61%	1.56%	0.64%	8.56%	54.31%	2.21%	0.13%	0.02%	0.93%
75	5.038	1.40E-02	0.25%	0.01%	31.15%	7.19%	0.52%	52.78%	3.26%	0.13%	0.89%	0.02%	3.83%
76	5.080	7.10E-02	0.02%	0.01%	86.72%	2.40%	0.26%	7.04%	1.86%	0.07%	0.05%	0.01%	1.57%
77	5.088	1.00E-03	0.05%	0.06%	14.99%	1.61%	2.25%	9.38%	66.25%	3.05%	0.26%	0.05%	2.06%
78	5.108	1.70E-02	0.08%	0.03%	17.33%	2.90%	2.16%	52.61%	19.77%	1.05%	0.31%	0.08%	3.68%
79	5.130	8.00E-03	0.02%	0.02%	4.56%	0.25%	0.96%	2.39%	86.97%	3.38%	0.67%	0.03%	0.76%
80	5.136	5.00E-03	0.02%	0.03%	4.01%	0.31%	0.93%	4.29%	86.69%	2.64%	0.48%	0.02%	0.60%